

AD-A056 994

AIR FORCE GEOPHYSICS LAB HANSCOM AFB MASS

F/G 3/1

AN OBSERVER'S MANUAL FOR THE AIR FORCE SWEPT FREQUENCY INTERFER--ETC(U)

FEB 78 K E EIS, R C RICKARD

UNCLASSIFIED

AFOL-TR-78-0048

NL

1 OF 1
AD
A056994



END
DATE
FILMED
9-78
DDC

AD A056994

AD NO. _____
DDC FILE COPY

LEVEL II

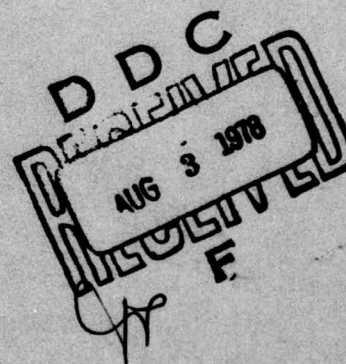
12
B.S.

AFGL-TR-78-0048
INSTRUMENTATION PAPERS, NO. 263



An Observer's Manual for the Air Force Swept Frequency Interferometric Radiometer

KENNETH E. EIS, Capt, USAF
RICHARD C. RICKARD, SSgt, USAF



21 February 1978

Approved for public release; distribution unlimited.

SPACE PHYSICS DIVISION PROJECT 4643
AIR FORCE GEOPHYSICS LABORATORY
HANSCOM AFB, MASSACHUSETTS 01731

AIR FORCE SYSTEMS COMMAND, USAF

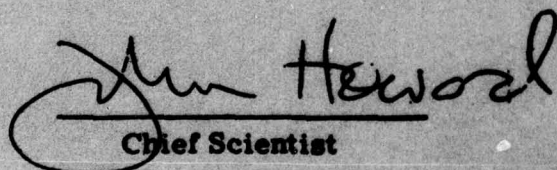


78 07 31 152

This report has been reviewed by the ESD Information Office (OI) and is releasable to the National Technical Information Service (NTIS).

This technical report has been reviewed and is approved for publication.

FOR THE COMMANDER


Chief Scientist

Qualified requestors may obtain additional copies from the Defense Documentation Center. All others should apply to the National Technical Information Service.

Unclassified
SECURITY CLASSIFICATION OF THIS PAGE (When Data Entered)

REPORT DOCUMENTATION PAGE		READ INSTRUCTIONS BEFORE COMPLETING FORM
1. REPORT NUMBER AFGL-TR-78-0048, AFGL-IP-263	2. GOVT ACCESSION NO.	3. REPORT'S CATALOG NUMBER
4. TITLE (and Subtitle) AN OBSERVER'S MANUAL FOR THE AIR FORCE SWEEP FREQUENCY INTERFEROMETRIC RADIOMETER.		5. TYPE OF REPORT & PERIOD COVERED INSTRUMENTATION PAPERS Scientific, Interim
7. AUTHOR(s) Kenneth E. Eis, Capt, USAF* Richard C. Rickard, SSG, USAF*		6. PERFORMING ORG. REPORT NUMBER
9. PERFORMING ORGANIZATION NAME AND ADDRESS Air Force Geophysics Laboratory (PH) Hanscom AFB, Massachusetts 01731		8. CONTRACT OR GRANT NUMBER(s)
11. CONTROLLING OFFICE NAME AND ADDRESS Air Force Geophysics Laboratory (PH) Hanscom AFB, Massachusetts 01731		10. PROGRAM ELEMENT, PROJECT, TASK AREA & WORK UNIT NUMBERS 62101F 46430305
14. MONITORING AGENCY NAME & ADDRESS (if different from Controlling Office)		12. REPORT DATE 21 Feb 1978
		13. NUMBER OF PAGES 1276 P.
		15. SECURITY CLASS. (of this report) Unclassified
		15a. DECLASSIFICATION/DOWNGRADING SCHEDULE
16. DISTRIBUTION STATEMENT (of this Report) Approved for public release; distribution unlimited.		
17. DISTRIBUTION STATEMENT (of the abstract entered in Block 20, if different from Report)		
18. SUPPLEMENTARY NOTES * AWS, Det 2, 12 Wea Sq The numerous examples of burst types included herein were recorded at the AFGL Sagamore Hill Solar Radio Observatory.		
19. KEY WORDS (Continue on reverse side if necessary and identify by block number) Solar meter bursts Interferometer Solar dekameter bursts Solar continuum activity Coronal radio bursts Sweep frequency receiver		
20. ABSTRACT (Continue on reverse side if necessary and identify by block number) This report describes the theory and equipment associated with the Sweep Frequency Interferometric Radiometer (SFIR). The report emphasizes data reduction and classification of the SFIR data. It is intended as a detailed manual to be used operationally, and as a training aid for those involved in reducing the SFIR data.		

DD FORM 1 JAN 73 1473 EDITION OF 1 NOV 65 IS OBSOLETE

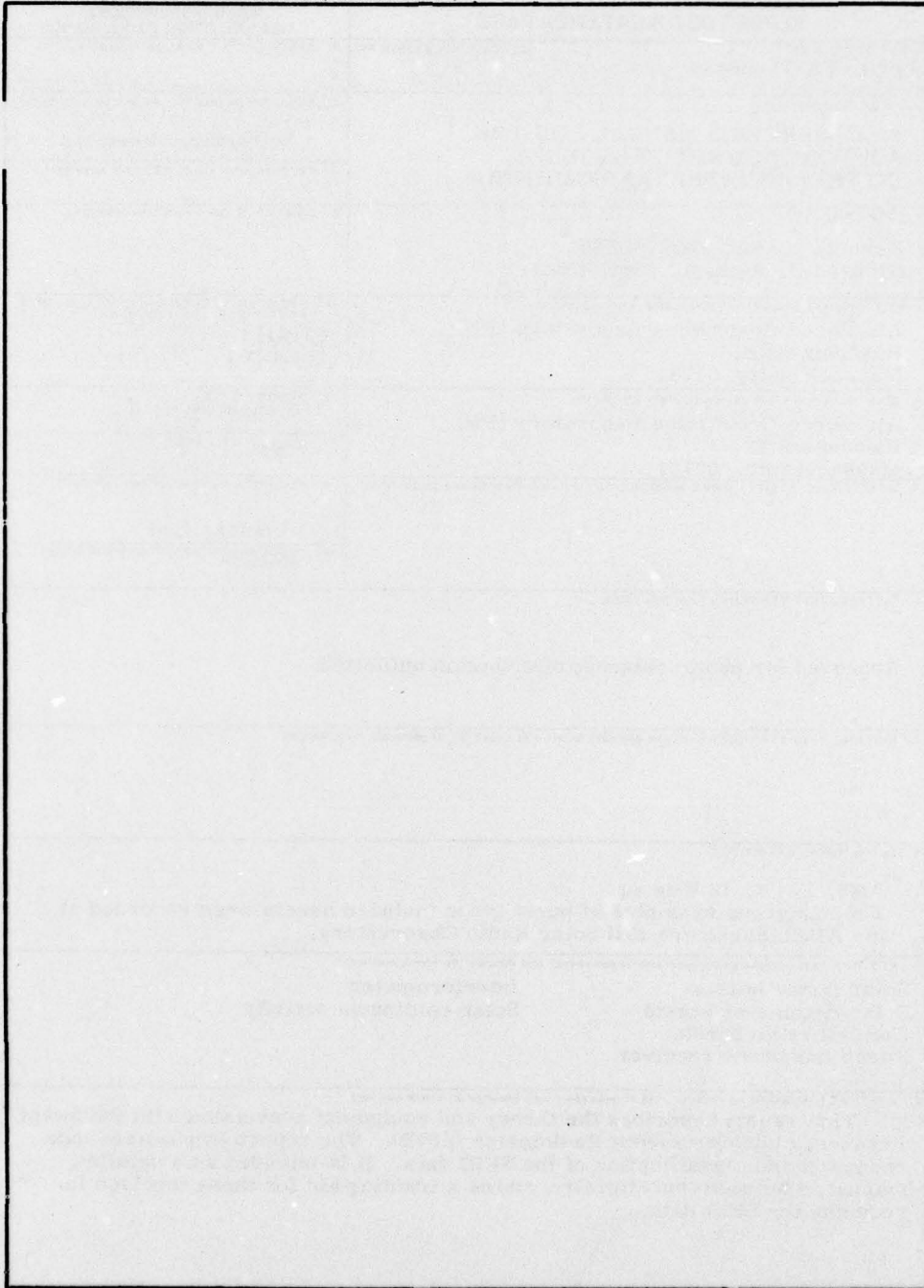
Unclassified
SECURITY CLASSIFICATION OF THIS PAGE (When Data Entered)

409578

78 07 31 152

hc

SECURITY CLASSIFICATION OF THIS PAGE(When Data Entered)



SECURITY CLASSIFICATION OF THIS PAGE(When Data Entered)

Preface

The authors would like to express their thanks to Mr. David Gaunt for his technical help on the instrumentation.

The authors would also like to thank Mr. John Castelli and Mr. Ronald Straka for their help and consideration, as well as Guy Tarnstrom for his many hours of discussion and clarification.

Special thanks are extended to SSgt Ronald Rains without whose active support this report would not have been possible.

ACCESSION for	
NTIS	File Section <input checked="" type="checkbox"/>
DDC	Book Section <input type="checkbox"/>
UNANNOUNCED	<input type="checkbox"/>
JUSTIFICATION	
BY	
DISTRIBUTION/AVAILABILITY CODES	
SPECIAL	
A	

Contents

1. INTRODUCTION	9
2. INSTRUMENTATION	10
2.1 Introduction	10
2.2 Interferometer Theory	10
2.3 Offset	15
2.4 Frequency Swept Interferometer	17
2.5 Physical Description of the SFIR and Data Output	18
3. THEORY OF SOLAR DEKAMETER BURSTS	23
3.1 Introduction	23
3.2 Solar Emission Theory or the Plasma Hypothesis	23
3.3 Mechanisms for Radio Emission Other than the Plasma Hypothesis	27
3.4 Classification of Sweep Frequency Solar Meter/Dekameter Bursts	27
3.4.1 Drift Frequency Bursts	27
3.4.1.1 Type II Bursts (Slow Drift)	28
3.4.1.2 Type III Bursts (Fast Drift)	29
3.4.1.3 Type V Bursts	30
3.4.2 Continuum Bursts	31
3.4.2.1 Type I Bursts	31
3.4.2.2 Continuum Storms	31
3.4.2.3 Type IV Bursts	32
4. DATA INTERPRETATION	32
4.1 Introduction	32
4.2 Logic Decision Chart for Burst Classification	33
4.3 Data Interpretation	35
4.4 Jupiter Bursts	39
4.5 Burst Classification Hints	69
4.6 Observational Hints	70

Contents

4.7 Total Power Trace Signature	71
4.8 Spectrum Analysis	72
5. FUTURE DEKAMETER/METER DEVELOPMENTS	74
BIBLIOGRAPHY	75

Illustrations

1. Block Diagram of Sweep Frequency Interferometric Radiometer	10
2. Interferometer, and Incoming Signal Geometrical Relationship	11
3. Difference in Signal at Antennas A and B	13
4. Interference Fringe Intensity vs Difference Signal	14
5. Schematic of Fringe Spacing During Observing Day (Without Delay Line)	15
6. Placement of Delay Line	16
7. Schematic of Fringe Spacing During Observing Day (With Delay Line)	16
8. Schematic of Fringe Spacing During Observing Day With Delay Line and Antenna Reversal at Noon ($\theta = 90^\circ$)	17
9. SFIR Semi-Bicone Antenna	18
10. SFIR Electronic Component Rack	19
11. SFIR Electronic Data Display	20
12. Solar Continuum Emission and Ionospheric Effect	21
13. Time Code Breakdown	22
14. Elevation of Iso-Frequency Surface Above Solar Active Region	24
15. Change in Critical Frequency vs Solar Height With Different Density and Magnetic Field Models	25
16. Schematic of Type I Burst	28
17. Schematic of Type II and Group of Type III Bursts	29
18. Schematic of Type V Burst With Group of Type III's	30
19. SFIR Data Sample-No Signal	40
20. Type V and Type III Solar Radio Burst	41
21. Type III and Type V Burst	42
22. Type V and Group of Type III's	43
23. Type V and Detached Type III	44
24. Type III and Group of Type III's	45

Illustrations

25. Three Groups of Type III's of Varying Intensities	46
26. Series of Type III's and Continuum	47
27. Type IV	48
28. Type II	49
29. Type IV, Group of Type III's and Continuum	50
30. Type V and Group of Type III's Plus Channels 4 and 12	51
31. Type V and Group of Type III's	52
32. Type V and Group of Type III's	53
33. Group of Type III's	54
34. Type V and Group of Type III's	55
35. Type V With Group of Type III's	56
36. Type IV	57
37. Type IV and "Off Fringe" Type III	58
38. Continuum	59
39. Type V With Group of Type III's	60
40. Type II With Group of Type III's	61
41. Type II With Type V and Group of Type III's	62
42. Type II With Type V and Group of III's	63
43. Classical Major Event With Type V and Group of Type III Followed by Type II and Type IV	64
44. Schematic Representation of Major Event Similar to Figure 38	65
45. Strong Type V and Group of Type III's	66
46. Strong Type V and Group of Type III's	67
47. Jupiter Burst	68
48. Geometry of Pre-Limb Dekameter Burst Activity With Respect to Earth Observation	70
49. Typical Total Power Signature	71
50. Total Power Trace 4 July 1974	72
51. Instantaneous Spectrum Analyzer Display Type II	73
52. Instantaneous Spectrum Analyzer Display Type IV	73

Tables

1. Critical Frequency, Height, Coronal Electron Density Table	26
---	----

An Observer's Manual for the Air Force Swept Frequency Interferometric Radiometer

1. INTRODUCTION

This technical report is intended to supplement AWSR 105-32, Chapter 7. Currently, no concise explanation of sweep frequency interferometry, data reduction, or theory exists for the solar radio observer to use as a reference. This is particularly critical at this moment because of the deployment of the Radio Solar Telescope Network (RSTN) which will include a sweep frequency interferometric radiometer (SFIR) as well as eight discrete frequency radiometers. Because of this deployment, all solar radio observers will have to evaluate and interpret SFIR data as well as the discrete frequency records.

This report includes actual data which will aid the observer in the interpretation of the SFIR data record. Other SFIR data appears in the current scientific literature, but differences in sensitivity and display format make the translation of this data by the inexperienced solar observer difficult.

This report will be divided into four sections: instrumentation, solar dekameter burst theory, data interpretation, and the current and future uses of dekametric information.

(Received for publication 21 February 1978)

2. INSTRUMENTATION

2.1 Introduction

The sweep frequency interferometric radiometer (SFIR) under discussion, an AFGL design, was initially a 24-MHz bandwidth device. In 1975, its bandwidth was modified to 50 MHz. The data from both of these modes of operation are represented in this report. A third configuration is a system designed by Cincinnati Electronics Corporation (CEC) specifically as part of the RSTN. The CEC device incorporates the same electronics and antenna systems as the AFGL system with slight modifications. The major difference between the AFGL and CEC systems is the display printer and the antenna reverse switch. These differences will be detailed in subsequent sections.

Fundamentally, the SFIR is the mating of two devices: an interferometer, and a sweep frequency radiometer. Since the theory of interferometry is independent of the theory of sweep frequency radiometers, the two functions will be explained separately.

2.2 Interferometer Theory

The interferometer is a device that senses radio emission from a source using two or more antennas. In the case of the AFGL SFIR at Sagamore Hill, two antennas, both detecting radio frequency electromagnetic radiation, are spaced 300 m apart. (See Figures 1 and 2.)

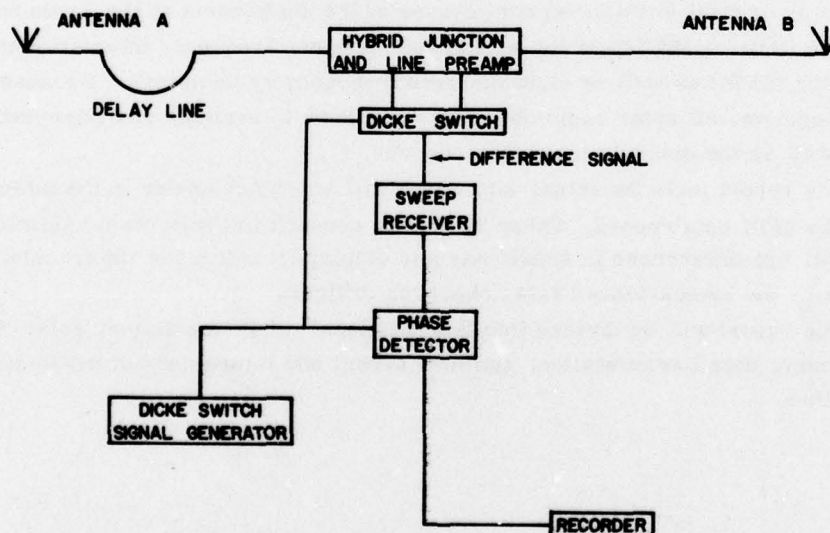


Figure 1. Block Diagram of Sweep Frequency Interferometric Radiometer

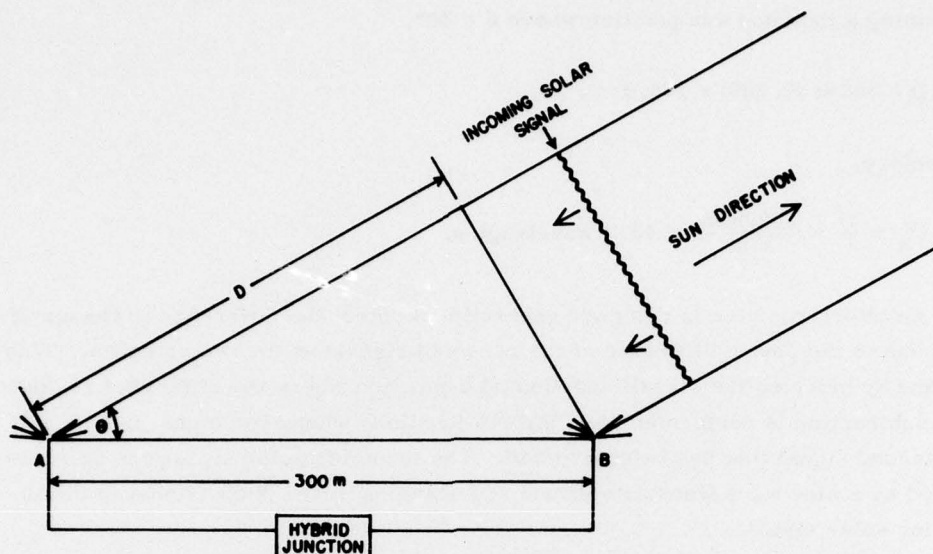


Figure 2. Interferometer, and Incoming Signal Geometrical Relationship

The antennas are oriented east-west so the angle θ in Figure 2 varies from 0° at sunrise, to 90° at local noon, to 180° at sunset. (Note that the north-south orientation of the sun does not effect this theory because of rotational symmetry about the antenna's baseline (AB). In Figure 2, an incoming signal from the Sun would have to travel a distance D further to get to antenna A, then to get to antenna B. This distance can be expressed in wavelengths.

Example:

If the interferometer were detecting a 50 MHz signal, the wavelength would be

$$\lambda = c/f, \quad (1)$$

where c is the speed of light, and f is the frequency of the signal. Substituting,

$$\lambda = \frac{3 \times 10^8 \text{ m/sec}}{5 \times 10^7 \text{ Hz}} = 6 \text{ m}.$$

The distance D is found from the equation

$$D = 300 \cos \theta. \quad (2)$$

Assuming a morning sun position where $\theta = 30^\circ$,

$$D = 300 \text{ m} (0.866) = 259.8 \text{ m}.$$

Therefore,

$$D_\lambda = \frac{D}{\lambda} = \frac{259.8 \text{ m}}{6 \text{ m}} = 43.3 \text{ wavelengths.}$$

An interferometer is designed generally to detect the difference in the amplitude due to the phase difference of the received signals at the two antennas. This is done by bringing the signals together at a junction where the difference is taken. The subtraction is performed by a "hybrid junction" where one signal is added to the second signal that has been inverted. The incoming solar signal can be represented by a sine wave whose amplitude and wavelength are proportional to the incoming solar signal.

In Figure 3, $D_\lambda = 8.5$. (If the baseline were still 300 m and $\theta = 30^\circ$, λ would be approximately 57.7 m.) The difference between the signal at antenna A and B is therefore E_O or the full peak-to-peak amplitude of the detected sine wave. The hybrid output would be maximum at a $D_\lambda = 8.5$ spacing because $E_A = -E_B$. The hybrid output is $V_O = E_A - E_B$. Substituting where $E_A = -E_B$ yields $V_O = 2E_O$, or V_O 's maximum value. Using the same reasoning, the interferometer output would be maximum at any point where $D_\lambda = (n + 0.5)\lambda$ where n is an integer. This is because the two signals are exactly out of phase. If $D_\lambda = n\lambda$, the output would be zero because the amplitude of the sine waves at the two antennas is equal and in phase; therefore, the difference is zero. Generally the interferometer output can be represented as

$$V_O = E_O (\sin \phi_A - \sin \phi_B), \quad (3)$$

where ϕ_A and ϕ_B are the phase angles of the incoming wave at antennas A and B. Since ϕ goes through 360° of rotation in one wavelength,

$$\sin \phi = \sin \phi \pm n (360^\circ). \quad (4)$$

If $\phi_A = \phi_B \pm n (360^\circ)$ in Eq. (3), the interferometer output V_O is 0. If ϕ_A and ϕ_B are $180^\circ \pm n (360^\circ)$ apart, V_O is maximum. On the other hand if ϕ_A and ϕ_B are $90^\circ \pm n (360^\circ)$ or $270^\circ \pm n (360^\circ)$ apart, V_O will be at half maximum. Since D_λ is in wavelengths and one wavelength corresponds to a 360° phase shift

$$\phi_A - \phi_B = D_\lambda (360^\circ). \quad (5)$$

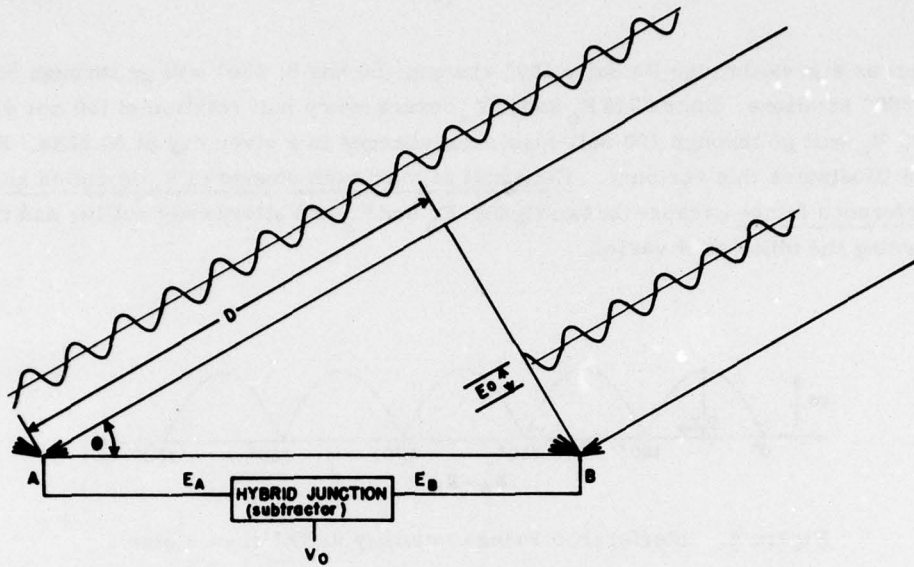


Figure 3. Difference in Signal at Antennas A and B

Combining Eqs. (5) and (3) yields

$$V_o = E_o [\sin (\phi_B + D_{\lambda} \cdot 360^{\circ}) - \sin \phi_B] . \quad (6)$$

Substitution of Eq. (2) yields

$$V_o = E_o [\sin (\phi_B + (\frac{300}{\lambda} \cos \theta) \cdot 360^{\circ}) - \sin \phi_B] . \quad (7)$$

Where again:

- V_o is the hybrid junction output,
- E_o is the detected maximum signal at either antenna,
- ϕ_B is the phase angle of the incoming wave at antenna B,
- and λ and θ are variables.

To illustrate the behavior of V_o set $\lambda = 6 \text{ m}$ (50 MHz) and $\phi_B = 0$. This yields

$$V_o = E_o \sin (50 \cos \theta \cdot 360^{\circ}) .$$

V_o will vary from 0 to E_o each time the quantity

$$(50 \cos \theta) 360^{\circ} \quad (8)$$

varies 180° ; which is a very small change in θ .

In fact as θ goes through its daily 180° change, $(50 \cos \theta) 360^\circ$ will go through 50 full 360° rotations. Since a 0 to E_0 and in V_0 occurs every half rotation of $(50 \cos \theta) 360^\circ$, V_0 will go through 100 null-maximum changes in a given day at 50 MHz. Figure 4 illustrates this variance. Each null to maximum change in V_0 is called an interference fringe because the two signals E_A and E_B are alternately nulling and re-enforcing the other as θ varies.



Figure 4. Interference Fringe Intensity vs Difference Signal

The interferometer display can detect fringe shifts of about $1/10$ of a fringe which corresponds to a phase angular change of $(180^\circ) 1/10 = 18^\circ$. Substitution into Eq. (8) yields

$$18^\circ = (50 \cos \theta) 360^\circ \text{ or,}$$

$$\Delta \cos \theta = \frac{1}{1000}.$$

This gives the angular resolution of the interferometer for an angular displacement $\Delta\theta$ at any angle θ made parallel to the interferometric baseline. At $\theta = 0$, $\Delta\theta = 0.1^\circ$, at $\theta = 30^\circ$, $\Delta\theta = 0.115^\circ$, and at $\theta = 90^\circ$, $\Delta\theta = 0.06^\circ$. 0.1° corresponds to about $1/5$ of a solar radius so if an eruptive prominence emitting 50 MHz radiation were to move one solar radius parallel to the interferometer baseline at local noon, the fringe pattern would shift approximately one full fringe.

Since the sun moves about 15° per hour, θ varies approximately at that rate. This causes a continuous fringe shift as illustrated in Figure 5.

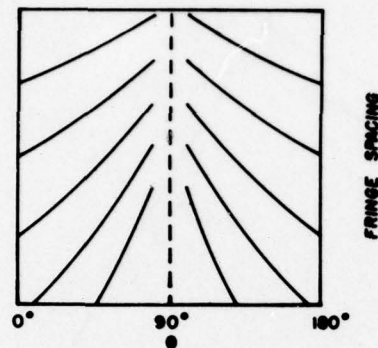


Figure 5. Schematic of Fringe Spacing During Observing Day (Without Delay Line)

2.3 Offset

Since the interferometer data record is made up entirely of fringes, there is a problem at local noon where $D = 0$. When this occurs (see Figure 5), no fringes appear on the record. To eliminate this problem, a method has been developed to stop D from ever reaching 0.

In Figure 6, the difference in the signal reaching the hybrid junction or subtractor circuit is not only due to D_λ but also due to the additional cable length D_w added to antenna A's transmission line. D_w is also in units of observed wavelengths. In this case Eq. (5) no longer holds but rather,

$$\phi_A - \phi_B = \left(D_\lambda + \frac{D_w}{\lambda} \right) 360^\circ, \quad (9)$$

so when $D = 0$, $\phi_A - \phi_B \neq 0$. D_w is selected to minimize fringe spacing and insure that D never goes to 0 at any time of day. Figure 7 shows the fringe spacing with the addition of D_w for the AFGL SFIR. The fringes become more closely spaced as the day progresses. Figure 8 shows the interference fringe behavior of the RSTN SFIR's developed by Cincinnati Electronics. Here the antennas, A and B, are electrically reversed at local noon to decrease the fringe shift spacing change during the day.

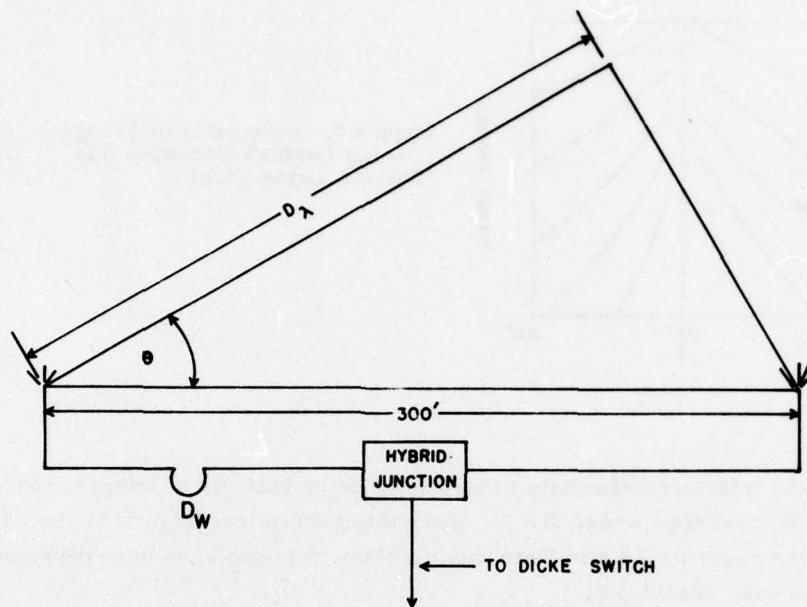


Figure 6. Placement of Delay Line

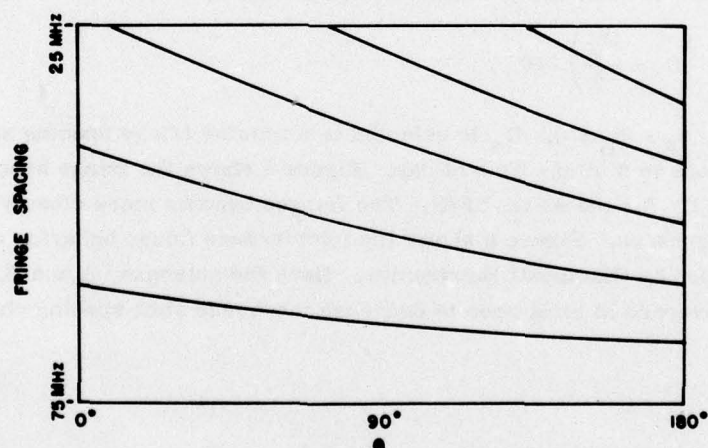


Figure 7. Schematic of Fringe Spacing During Observing Day (With Delay Line)

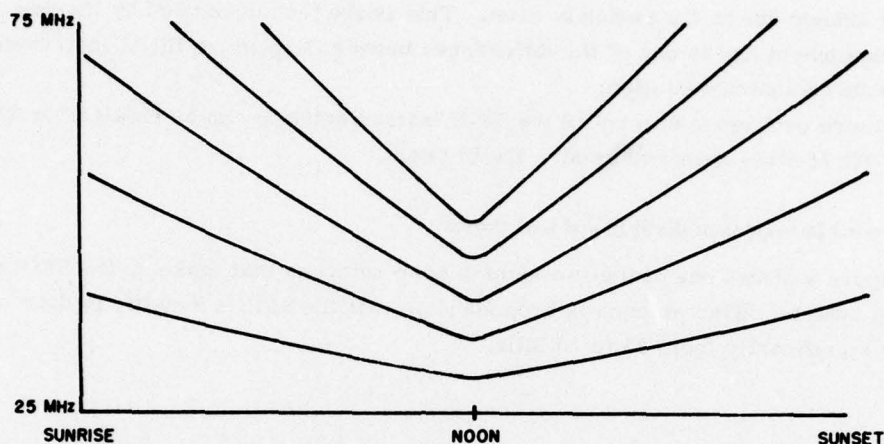


Figure 8. Schematic of Fringe Spacing During Observing Day With Delay Line and Antenna Reversal at Noon ($\theta = 90^\circ$)

2.4 Frequency Swept Interferometer

V_o also varies if θ is held constant and λ is allowed to vary. This pattern of V_o is identical to Figure 4 since V_o still varies as a sine function.

As an example, when $\theta = 89^\circ$ (just before local noon) where $\cos 89^\circ = 0.0175$, Eq. (7) can be written

$$V_o = E_o \left[\sin \left(\phi_B + \frac{5.24}{\lambda} \cdot 360^\circ \right) - \sin \phi_B \right].$$

Again letting $\phi_B = 0$ yields,

$$V_o = E_o \sin \left(\frac{5.24}{\lambda} \cdot 360^\circ \right).$$

As λ varies from 4 to 12 m, $5.24/\lambda$ varies from 1.3 to 0.44 which is almost a full 360° . Because of this, V_o will vary through a fringe pattern because of the frequency shift as well as the change in θ .

Figure 7 illustrates the fringe pattern change during one observational day with a delay line inserted. Furthermore, at any given θ , there is also a fringe pattern. For instance, at $\theta = 90^\circ$ the frequency sweep causes four fringes to be exhibited on the display in Figure 7.

Figure 8 illustrates the fringe pattern that would result if the antenna were reversed east to west at local noon. This allows the number of fringes to remain more nearly constant throughout the day due to the 50 percent decrease in the

angle θ change due to the switch at noon. This is the technique used by the new RSTN equipment and is one of the differences between Sagamore Hill's instrument and the RSTN instrumentation.

A more detailed treatment of the SFIR instrumentation can be obtained in AFGL report TR 76-0194 authored by Mr. David Gaunt.

2.5 Physical Description of the SFIR and Data Output

Figure 9 shows one of the two semi-bicone antennas that make up the SFIR's antenna system. This antenna is broadband so that the SFIR's sensitivity does not change significantly from 25 to 75 MHz.



Figure 9. SFIR Semi-Bicone Antenna

Figure 10 illustrates the electronics of the SFIR. The top panel is the tracking generator used for calibration. The next instrument is the Hewlett-Packard Spectrum Analyzer which is used as the swept frequency receiver. Below the receiver is the antenna reversing switch control panel. At the very bottom is a voltage regulator.

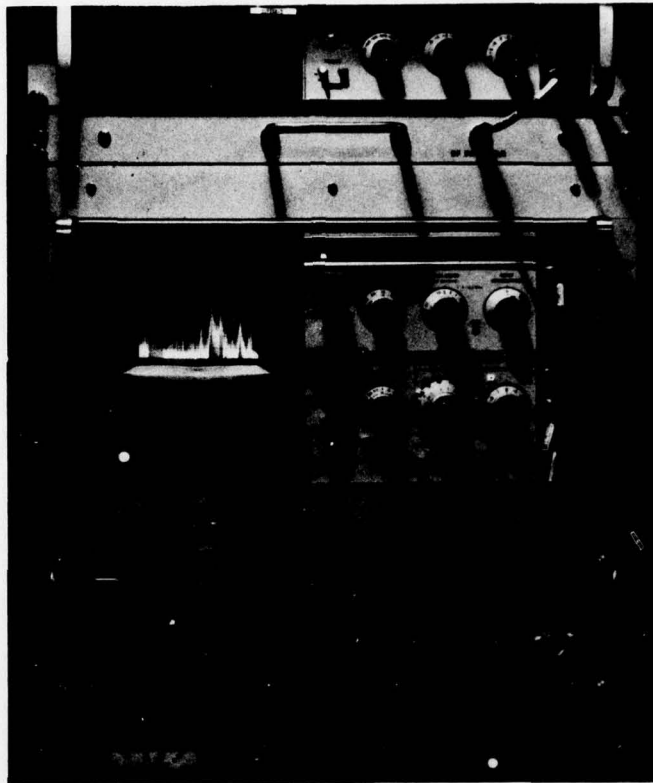


Figure 10. SFIR Electronic Component Rack

Figure 11 is the electrostatic display device for the SFIR. The paper feeds from bottom to top and the frequency sweeps from 25 MHz (left edge of the paper) to 75 MHz (the right edge of the paper).

Figure 12 illustrates typical data from the Sagamore Hill SFIR. Notice the fringe patterns which show up as fuzzy dark lines that drift from higher to lower frequencies in time. Warning: Data generated by the Sagamore Hill SFIR (all of the data in this report) has time increasing to the top. The new RSTN data runs increasing time down. This difference should be kept in mind whenever the examples are applied to any particular observatory as guidance.

A 10 - 15 min delay in the data interpretation results from the physical position of the printing head in the electrostatic printer. It takes this long for the paper at the print head to emerge from the printer sufficiently to be seen by the observer.

Figure 12 also illustrates the time code and one minute marker lines common to both display arrangements. Figure 13 shows the detailed time code breakdown.

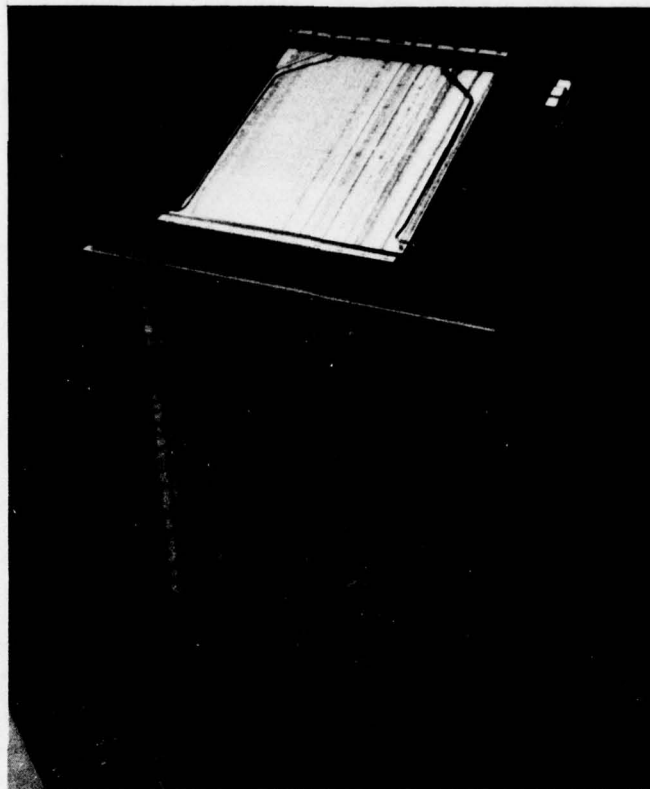
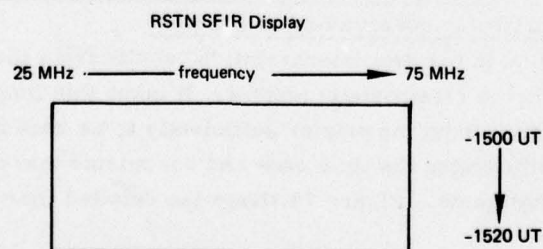
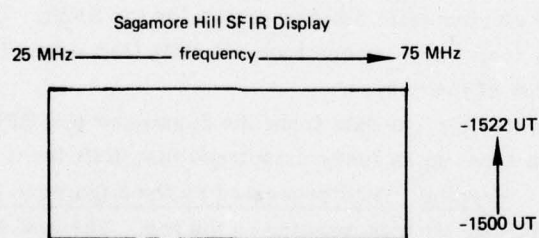


Figure 11. SFIR Electronic Data Display



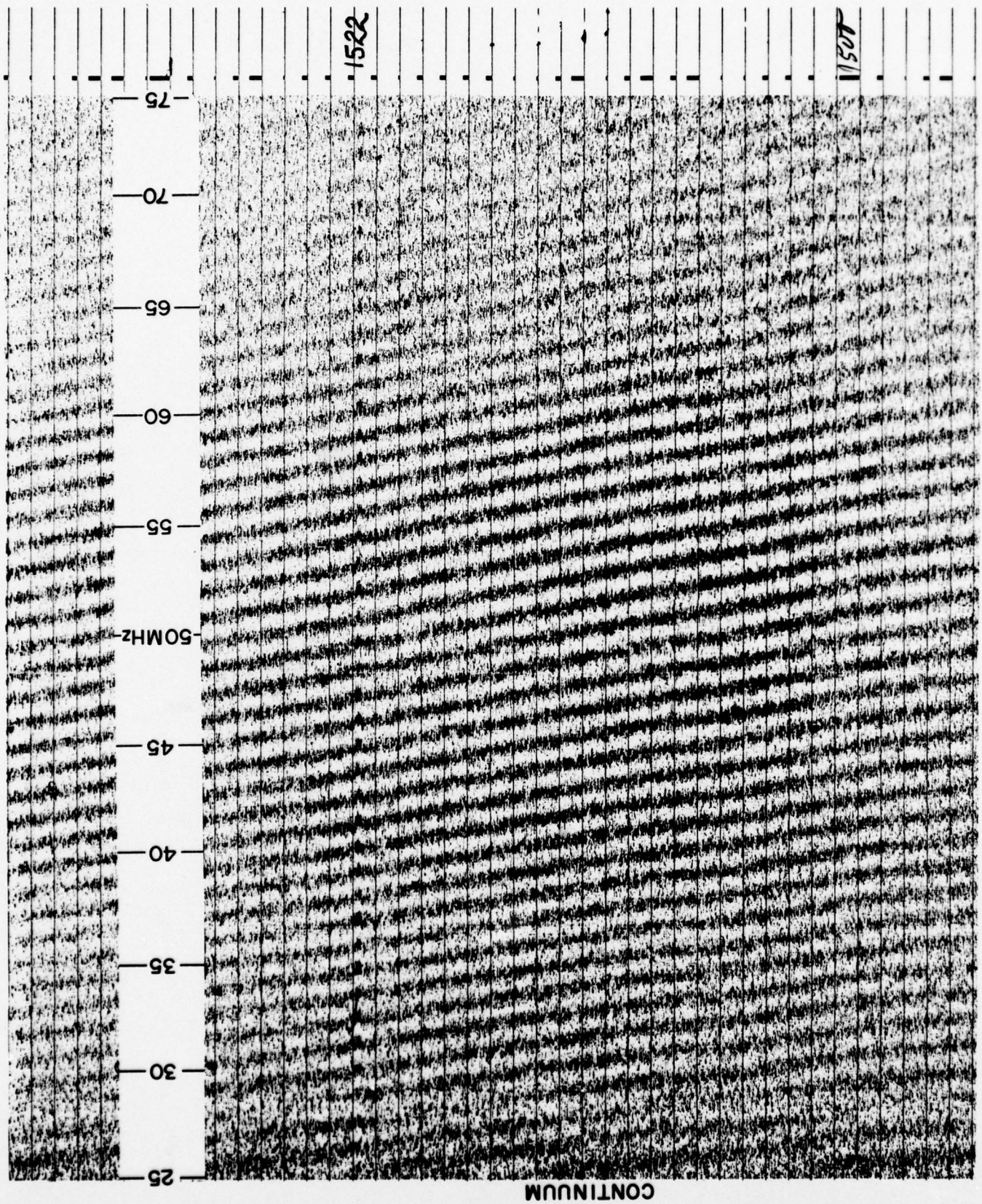


Figure 12. Solar Continuum Emission and Ionospheric Effect

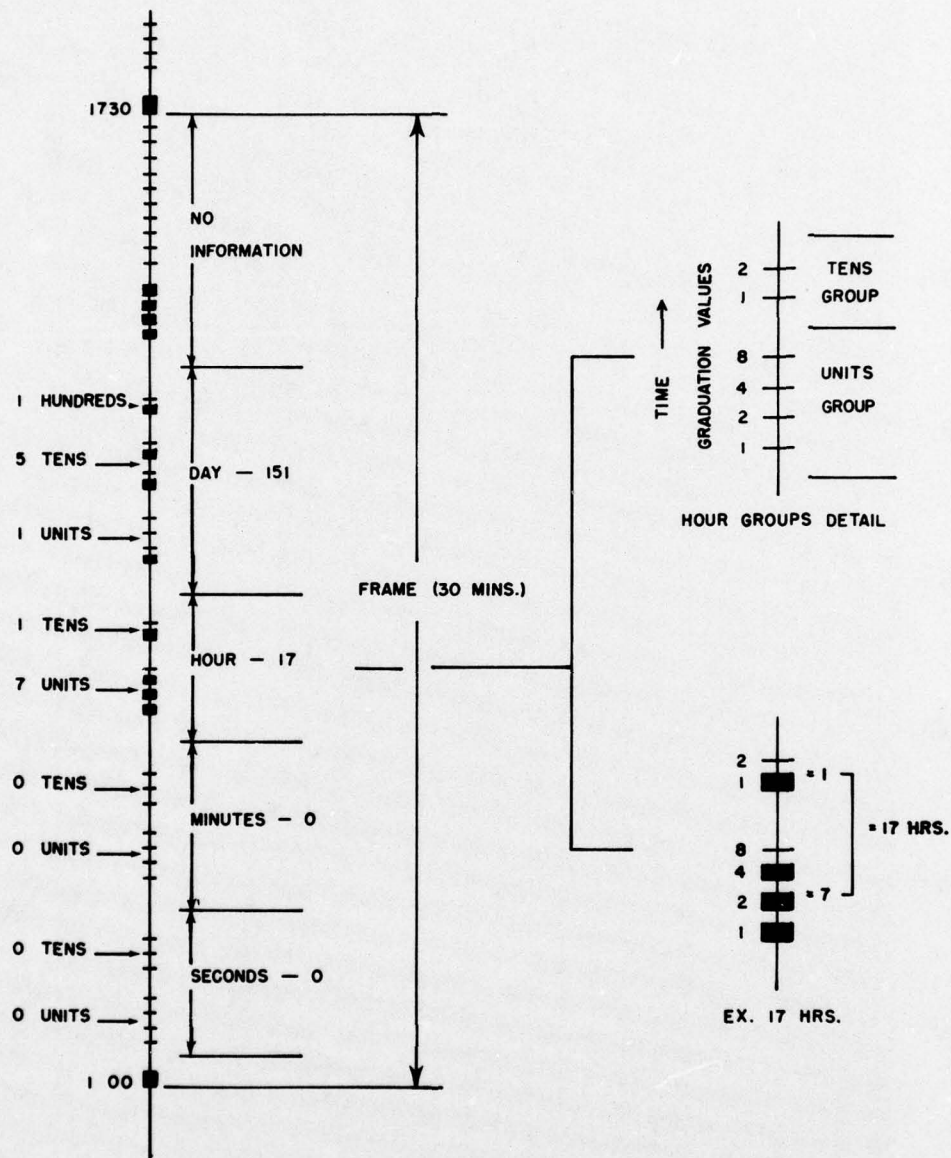


Figure 13. Time Code Breakdown

3. THEORY OF SOLAR DEKAMETER BURSTS

3.1 Introduction

The study of solar observations in the meter and dekameter (tens of meters) region of the radio spectrum can be divided into the theory of radio emissions and the classification system of dekameter bursts. The classification system devised by solar physicists in the 1950's is the same system used by AWS observers to report bursts in the 25 MHz to 75 MHz region and should therefore be well understood by all certified AWS solar radio observers. The theory of radio emission is intrinsically complicated. Only the basics of the plasma hypothesis and other emission theories will be presented. If a more detailed explanation is needed, one of the texts in the bibliography should be consulted.

3.2 Solar Emission Theory or the Plasma Hypothesis

J. P. Wild, an Australian solar physicist, first proposed the plasma hypothesis in 1950. The theory basically states that an ionized plasma when excited by mechanical, electrical, magnetic, or thermal means will radiate radio noise at a frequency defined by equations dependent upon the following variables:

- (1) N —The electron density (electrons per cubic meter),
- (2) H —The magnetic field strength and direction (gauss)
- (3) γ —The collision frequency of electrons with heavy ions
(number per volume per second).

Two of the basic formulas are:

$$f_o = \sqrt{\frac{N_e}{\pi m}}, \quad (10)$$

and

$$f_H = \frac{eH}{2\pi mc} \quad (11)$$

where f_o is called the plasma frequency and f_H the gyrofrequency. The other symbols in these equations represent constants which are:

- e = electron's electric charge, 1.6×10^{-19} esu,
- m = mass of the electron 9×10^{-31} Kg,
- c = speed of light, 3×10^8 m/sec.

The signal f_o illustrates that an ionized gas with an electron number density of N will naturally oscillate. Equation (10) indicates that, as the density drops, so does f_o .

Since the sun's atmosphere is made up entirely of ionized gases whose density decreases with height, the lower plasma frequencies are generated at higher altitudes. In the presence of a magnetic field an ionized plasma oscillates at a natural resonance frequency defined by Eq. (11). The coronal electron density N is given by Figure 15. The natural plasma frequency is thus dependent upon the magnetic field strength and electron density, which both decrease with increasing height. Because of this, lower frequencies tend to be generated by higher layers of the sun's atmosphere. In regions containing strong magnetic fields, the constant frequency level is raised above the mean level as illustrated in Figure 14. This effect is analogous to the isobaric surfaces in the earth's atmosphere being depressed in elevation over a surface cold core low and elevated over a surface warm core high. Continuing this analogy, solar active regions, which are also regions of enhanced magnetic intensity, correspond to surface highs. Table 1 is a numerical illustration of Figure 15 showing the different results obtained when different density-vs-height relationships are used.

The plasma hypothesis also states that harmonics can be generated. As an example, if the solar corona were stimulated at a height of 900,000 km (see Table 1 and Figure 15) the fundamental frequency generated would be 10 MHz, but additionally, the 2nd harmonic at 20 MHz, and the 3rd harmonic at 30 MHz could be produced.

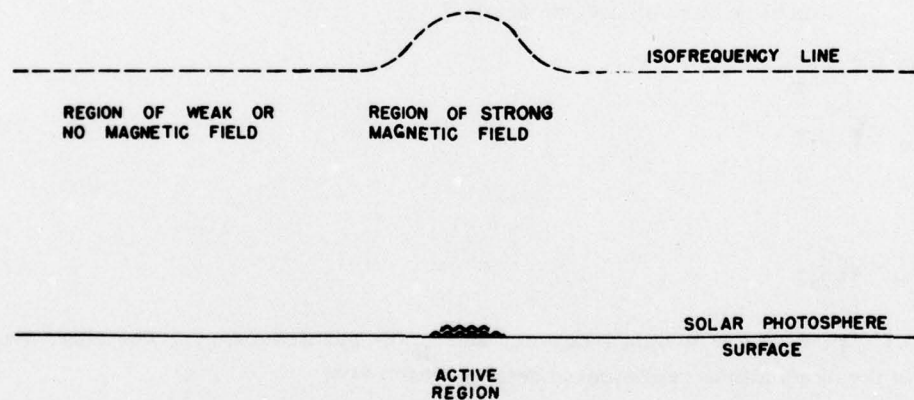


Figure 14. Elevation of Iso-Frequency Surface Above Solar Active Region

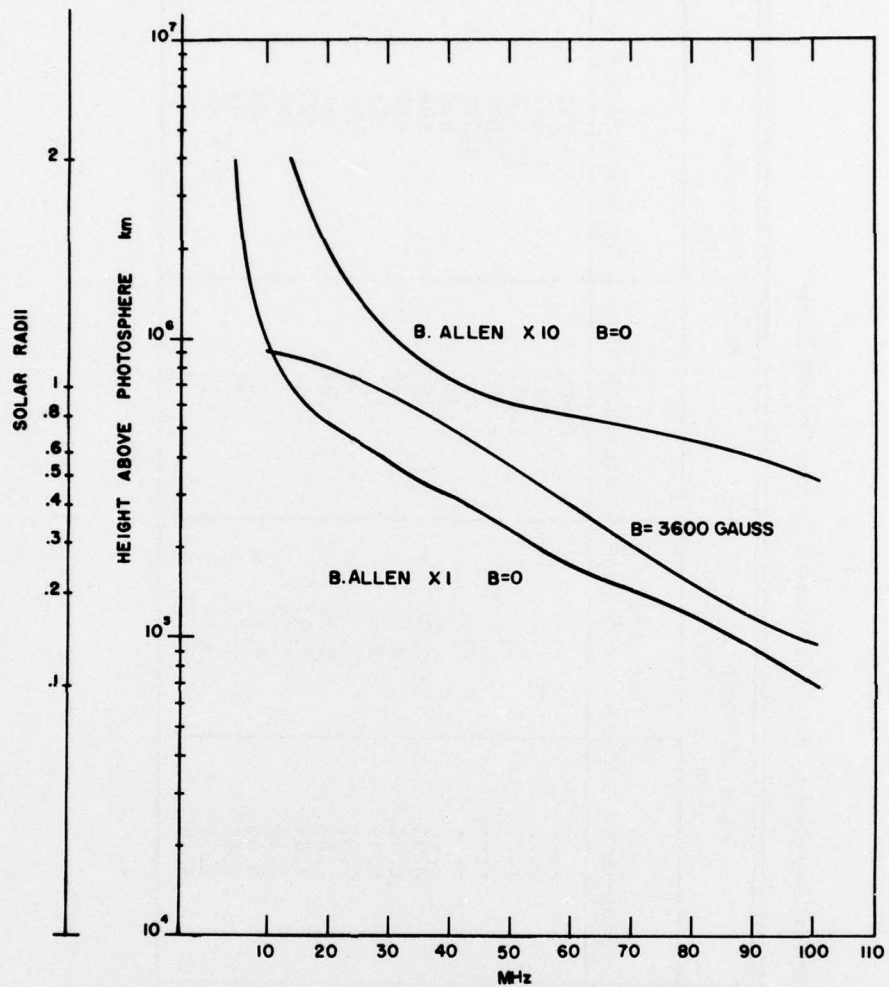


Figure 15. Change in Critical Frequency vs Solar Height With Different Density and Magnetic Field Models

An area of controversy in the plasma hypothesis is the physics of stimulation. Clouds of relativistic and non-relativistic electrons and shockwaves are considered the stimulating agents, but the method by which they actually interact with the coronal plasma to generate the radio waves is still a subject of controversy.

Table 1. Critical Frequency, Height, Coronal Electron Density Table

Height Above Photosphere $\times 10^3$ km	Distance Above Surface in Solar Radii	Electron Density (Log N cm ⁻³)		Plasma Frequency MHz	
		Baumbach Allen	Max. Above Active Regions	Baumbach Allen	Baumbach Allen $\times 10$
0.5	.0007	6,808	21,513
1.0	.0014	5,615	17,743
2.0	.0029	3,821	12,074
4.0	.0058	1,769	5,591
6.0	.0086	819	2,588
10.0	.0144	176	556
20.9	.03	8.51	9.06	160	506
41.7	.06	8.36	8.96	136	430
69.5	.1	8.19	8.82	111	351
139	.2	7.84	8.53	74	234
209	.3	7.56	8.25	54	171
278	.4	7.34	8.01	42	133
348	.5	7.15	7.79	34	107
417	.6	6.96	7.59	28	88
556	.8	6.66	7.23	19	60
695	1.0	6.38	6.95	14	44
1390	2.0	5.33	4.3	14

3.3 Mechanisms for Radio Emission Other than the Plasma Hypothesis

Two other methods of radio wave generation are used to explain certain solar radio emissions.

Bremsstrahlung is a German word meaning "breaking radiation". This breaking radiation results when electrons moving about randomly in an ionized gas deflect each other due to the interaction of their electric fields, thus producing radio waves, visible light, and possibly X-rays, depending upon how strongly they interact. This generation mechanism is also credited with producing the thermal or quiet sun radiation measured as IFLUX by AWS observers. The second method of propagation is gyrosynchrotron emission. Here the electron emits radiation as it is deflected by the solar magnetic field.

3.4 Classification of Sweep Frequency Solar Meter/Dekameter Bursts

The AWS classification scheme for reporting and archiving bursts is the same classification system used by a majority of the scientific community. This classification system is presented in a concise manner in the Descriptive Text of NOAA's Solar Geophysical Data bulletin as well as in many articles in the scientific literature. (See bibliography.) The scheme basically uses the burst's behavior in time and frequency to determine which burst type is present. This classification scheme is in contrast to the discrete frequency burst scheme which uses the intensity-time profile for determining the burst's classification.

The sweep frequency classification system consists of five general classifications normally seen by the AWS/AFGL SFIR. These are Type II, Type III, Type IV, Type V, and Continuum. The Type I noise storm will only be briefly covered because of its low probability of detection on the AWS instrument.

These five general classifications can be divided into two major subdivisions; drift frequency bursts, and continuum bursts.

3.4.1 DRIFT FREQUENCY BURSTS

There are two types of drift frequency bursts; slow and fast drift. Both types of bursts are generated by an excitation mechanism propagating through the solar corona from low to high altitudes. The mechanism stimulates the ambient plasma to generate radio waves at that level where f_o is generated (see Eq. (10)). As the agent moves from lower to higher altitudes the frequencies generated sweep from higher to lower frequencies. The stimulating agent has a sharp boundary and a limited size so the frequencies normally show an abrupt start and slightly less abrupt end. The agent can decay, decelerate or turn and re-enter the lower regions of the solar corona.

3.4.1.1 Type II Bursts (Slow Drift)

Type II bursts are believed to be caused by a shock wave acting as the excitation mechanism. The shock is possibly associated with the optically observed "Morton" wave that appears in H_{α} moving away from a flare site.

Type II bursts are generally easy to identify by their observed characteristics. These characteristics include:

Frequency Drift - Type II's can have frequency drifts from 0.05 MHz per sec to 1 MHz per second. Translated into the SFIR's 50-MHz bandwidth, this means that the leading edge or burst center can take 1 min to 16 min to go from 75 to 25 MHz. The drift rate can decrease during an individual burst and usually does. This is usually explained by the decreasing density gradient with altitude of the ambient coronal electrons through which the shock is moving.

Duration - Type II's usually have a total duration of 5 to 10 min while the single frequency duration is shorter and split into bands.

Harmonics - Type II's will, more often than not, show a harmonic and split band structure. (See Figure 16.) The splitting is normally from 5 to 10 MHz in the SFIR's frequency domain.

Correlation - Type II's are one of the rarer meter/dekameter bursts, normally associated with large flares and cm radio bursts. They are normally observed in conjunction with Type IV bursts which are also correlated with major solar activity.

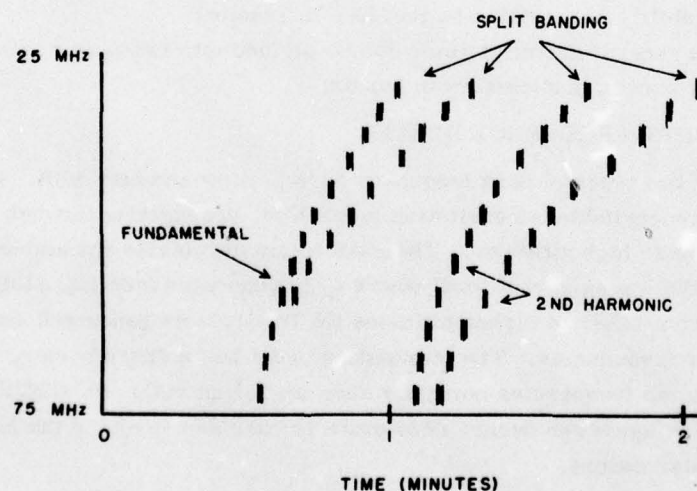


Figure 16. Schematic of Type I Burst

3.4.1.2 Type III Bursts (Fast Drift)

Type III's (see Figure 17) have a stimulating mechanism, believed to be electron swarms, moving at a much faster velocity than the shock associated with Type II's. The electrons generate radio frequency emissions by a mechanism, called coherent scattering. These electrons have been physically detected in the earth's vicinity.

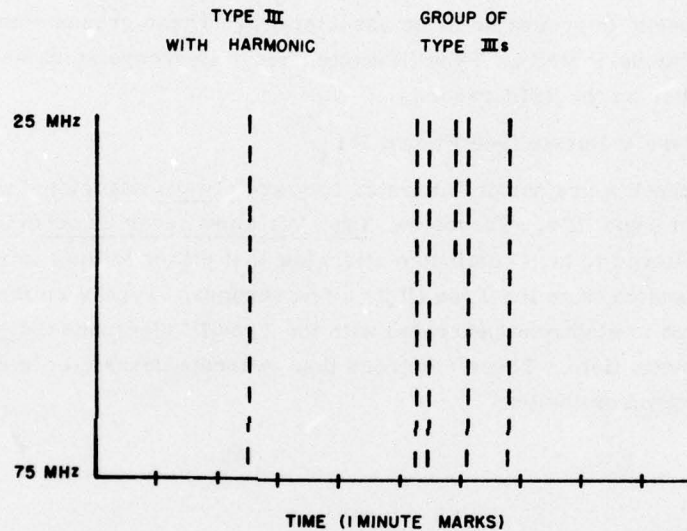


Figure 17. Schematic of Type II and Group of Type III Bursts

Frequency Drift - Since the electrons associated with Type III's are nearly relativistic (close to the speed of light), they move through the corona in a few seconds. Observed drift rates are between 1 and 70 MHz per second. The drift rates are in fact so fast that they are not measurable with the SFIR but rather appear as a burst beginning simultaneously at all frequencies. The appearance of "simultaneous turn on" is due to the 1 sec sweep rate of the SFIR and the 50-MHz bandwidth. In order to see the drift rate, the time resolution of the SFIR would need to be speeded up by a factor of 10. This is precluded by monetary and receiver sensitivity considerations.

Frequency Extent - Type III's usually extend over the entire SFIR bandwidth and can extend from 8 to 600 MHz or more. (The 8-MHz limit is the earth's atmospheric cutoff point. Experiments on board satellites have detected bursts extending into the KHz region.)

Duration - Type III's last only 1 or 2 sec because of the velocity of the electrons. Because of this short duration, they would be missed by the SFIR if they didn't often have harmonic structure and occur in groups.

Harmonics - Type III's normally occur with a 2nd harmonic. (This feature, unlike the Type II harmonic, is not discernable with the SFIR, but does extend the lifetime of the Type III to allow its detection by the SFIR.)

Correlation - Most Type III's occur during the lifetime of a flare. Unfortunately most of these flares were of the OF category.

Occurrence - Type III's are the most common of all dekameter/meter bursts. They normally occur in groups or loose associations. These groups sometimes have a marked, regular periodicity. Type III's often occur in groups so closely spaced they blend together on the SFIR record.

3.4.1.3 Type V Bursts (See Figure 18)

Although Type V's are not drift bursts, they are always associated with Type III's or groups of Type III's. Therefore, Type V's must never be reported alone. Type V's are believed to be a continuum afterglow that either follows immediately after, or is separated from the Type III by a few seconds. Type V emission is believed to be due to electrons generated with the Type III electrons that are trapped in a closed magnetic field. These electrons then generate dekameter/meter radio noise by synchrotron emission.

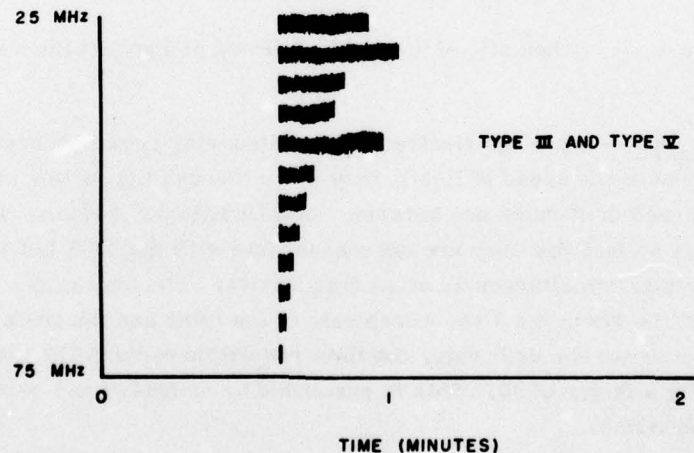


Figure 18. Schematic of Type V Burst With Group of Type III's

Duration - Type V's last from tens of seconds to several minutes. They generally are longer-lived at lower wavelengths.

Frequency Extent - Type V's can occur over the full 50-MHz bandwidth although they often show a sharp high frequency cut-off. This cut-off usually occurs above 75 MHz.

Intensity - Type V's can be one of the most intense bursts observed. They are generally more intense than III's or groups of III's because synchrotron emission is a more efficient generation mechanism than the coherent scattering mechanism responsible for Type III's.

Harmonics - Type V's do not have harmonic structure.

3.4.2 CONTINUUM BURSTS

Continuum bursts are bursts that generally have wide bandwidths and last for several minutes, hours, or days. They are not impulsive in nature or appearance.

3.4.2.1 Type I Bursts

Type I's are closely associated with the noise storms observed at 245 and 410 MHz. Type I's generally occur between 200 and 100 MHz so they are not observed on the 25 - 75 SFIR. Type I's show structure that lasts only a few seconds. Because of these characteristics, Type I's are not detectable with the Air Force SFIR and will therefore not be covered in any more detail.

3.4.2.2 Continuum Storms

The theoretical interpretation of a continuum is still subject to argument in the scientific community. Generally, continuum bursts are believed to be caused by either electrons leaking into the corona, which cause many unresolvable Type III like emissions, or possibly by a synchrotron emission mechanism.

Duration - Continuum lasts from tens of minutes to days. It can be the longest lasting of dekameter/meter activity.

Harmonics - A continuum has no harmonics.

Frequency Extent - The continuum can cover the entire 25 - 75 MHz SFIR band. However, the continuum can show a cut off at either end within the SFIR bandwidth.

Features - Continuum emission always shows structure. The structure appears as a weak continua background with many Type III like bursts imbedded within it. Sometimes the entire continuum will appear as a closely packed, sporadically intensifying Type III storm. Some scientists believe groups of Type III's evolve into continuum emission with no clear boundary separating them. Continuum structure generally takes on the appearance of patchy intensification "fuzzy Type III's" and a slowly increasing or decreasing bandwidth.

3.4.2.3 Type IV Bursts

Type IV's, like Type II's, are rare and associated with a major solar disturbance. Generally, it is believed that IV's are caused by a large number of electrons spiralling in the solar magnetic field and emitting radio frequencies by geosynchrotron or synchrotron emission.

Frequency Extent - Type IV's occur over the entire 25 - 75-MHz SFIR band. Type IV's can emit frequencies on into the centimeter wavelength band.

Duration - Typically IV's last 10 minutes. They can last days.

Features - Type IV bursts are recognized for their lack of features. They are broadband, slowly varying in intensity, with no internal structure.

Correlation - Type IV's are associated with major solar activity although the associated activity may be beyond the optical limb and therefore not observable on other sensors.

4. DATA INTERPRETATION

4.1 Introduction

In this section, schematics of bursts' details as well as photographs of actual bursts taken with the Sagamore Hill SFIR will be used to show how to interpret and classify dekameter/meter bursts. A logic decision table is also provided that illustrates a practical method of burst classification. Before examples are presented, the AWS classification system from AWSM 105-24, Volume II, paragraph 2-2 is reviewed.

T

- 2 - Type II (slow drift)
- 3 - Type III burst or group with duration of less than 10 seconds
- 4 - Type IV (smooth broadband continuum)
- 5 - Type V with Type III(s),
- 6 - Group of Type III's, from 10 sec to 30 min duration,
- 7 - Series of Type III's, or Group of Groups of Type III's, loosely associated, whose duration is greater than 30 minutes,
- 8 - Continuum (broadband continuum with Type III-like bursts superimposed),
- 9 - Unclassified.

Since Groups of Type III's can possibly turn into continuum emission, the distinction between codes 6, 7, and 8 is very tentative and will be discussed later.

4.2 Logic Decision Chart for Burst Classification

The logic decision scheme presented below should be used as an aid and not as the "one and only" means of dekameter burst classification. Like any scheme devised to classify nature, its logic is conditional and can therefore break down. Bursts are rarely sharply defined as one class vs another. Therefore, nothing will replace a well informed observer's judgement.

A. Does the burst have a clearly defined start? (Is the time from when you first detected the burst to full intensity less than 0.1 min), and does this start time not vary more than 0.1 min from the highest to lowest frequencies observed?

Yes - go to B

No - go to M

B. Does the burst last less than 0.1 minute?

Yes - you have a Type III

No - go to C

C. Are all of the following conditions met simultaneously?

1. Is the termination at all frequencies abrupt (like the beginning of a Type III)?

2. Are the end times at all frequencies such that a straight line can be drawn that coincides with it to within 0.1 minute?

3. Are all the end times within 0.2 minute?

Yes - go to D

No - go to J

D. Is the burst a discontinuous series of short duration bursts with no detectable fringe between the bursts?

Yes - go to E

No - go to I

E. Is the duration less than 15 minutes?

Yes - you have a group of Type III's

No - go to F

F. Is the duration less than 1 hour?

Yes - you have a series of Type III's

No - go to G

G. Is there a noise storm on the 245-MHz discrete frequency radiometer?

Yes - you have a continuum

No - go to H

H. Are the short duration bursts diffuse in their start and end?

Yes - you have a continuum

No - you probably have a long lasting series of Type III's

- I. Is the duration less than 30 minutes?
 Yes - you have a group of Type III's and a Type V
 No - you have a continuum
- J. Is the burst less than 10 min at all frequencies?
 Yes - you have a Type V and a group of Type III's
 No - go to K
- K. Is the burst associated with a large cm wavelength burst and flare?
 Yes - you have a Type IV
 No - go to L
- L. Does the total power indicate a rapid rise to greater than 50 sfu intensities?
 Yes - you have a group or series of Type III's and a Type V
 No - you have a continuum
- M. Does the burst have a clearly defined start (is the time from where you first detected the burst to full intensity less than 0.1 min) and does the start time vary to later times with decreasing frequencies?
 Yes - go to N
 No - go to O
- N. Is the burst associated with a major solar event?
 Yes - you have a Type II
 No - you have a continuum
- O. Is the burst associated with a major solar event and does the burst show no burst-like structure in its intensity or on the total power channel?
 Yes - you have a Type IV
 No - go to P
- P. Does the burst show superimposed Type III-like bursts? (On the electrostatic or total power display?)
 Yes - you have a continuum
 No - go to Q
- Q. Is the burst associated with a very weak noise storm on the low frequency discrete radiometers?
 Yes - you have a continuum
 No - go to R
- R. Is the burst so weak that it shows no deflection on the total power channel, very weak fringes and fringes that cover a small portion of the 75 - 25 MHz spectrum?
 Yes - you have a continuum
 No - you have a Type IV

Caution should be taken when the region producing the activity is beyond the limb of the Sun. The logic chart was created assuming the radio source was in full view; that is, not beyond the optical limb. If this assumption is not true, the logic chart may fail. The observational assumption is that the burst observed was on the disk

of the Sun. This assumption is often incorrect since the SFIR can see over the solar horizon. If this assumption were incorrect, it would affect the logic chart in the following ways:

- (a) Logic step G—Since the active region is beyond the limb of the Sun, the 245-MHz noise storm may be blocked by the limb,
- (b) Logic step K—Again, if the limb is blocking the chromosphere and lower corona from view, a large flare and high frequency radio burst may be presented but blocked from view by the limb of the Sun.
- (c) Logic step N and O—Here the same situation applies. The flare and high frequency burst activity is shielded from view by the edge of the Sun. Remember that the Type II and IV are still associated with a major solar event. Unfortunately, the event in question is not detected by anything but the SFIR.

4.3 Data Interpretation

The observer can learn the logic decision chart best by employing it with actual data records. He should always keep in mind the burst type characteristics presented in Section 3.4 as he classifies a burst. The first example, Figure 19, is an example of no data. The observer should notice two things:

- (a) There is no evenly spaced fringe pattern present. (Evenly spaced in frequency.)
- (b) There is no single frequency signature which drifts in frequency away from the time markers with time. As mentioned in Section 2.2, all solar bursts show a drift of their fringe patterns in time, if the bursts last long enough. This is the only rule the observer can absolutely count on. If it does not drift in time, it isn't solar in origin. Even Type III's, which are individually too short lived to show detectable drift, will show drift when they occur in closely spaced groups. Single frequency noise does appear at 67 and 72 MHz. To help orient the observer, he should hold all data records so that the time code is on the right. In this way, time increases up, and the left hand limit of the data corresponds to 25 MHz. The binary code blocks are outside the data domain and a new block is generated every 30 min (see Figure 13). The evenly spaced parallel lines are time lines which are generated every minute, exactly on the minute.

Figure 20 is an example of a Type III with a Type V. This can be determined by using the logic scheme:

- (a) The burst has a clearly defined start at 1454 UT,
- (b) The burst lasts longer than 0.1 min; it lasts until 1455 UT,
- (c) The burst does not have a rapid end at all frequencies; that is, it ends at 1455 UT at the low frequencies and at 1454.1 UT at 50 MHz,
- (d) The duration is less than 10 min, so logic step J indicates we have a Type V and a group of Type III's.

Figure 20 also shows channel 4 as the multiple banding between 67 and 75 MHz. Notice that no fringe shift is apparent with this banding whereas the Type V, although short lived, does show a fringe shift.

Figure 21 is a Type V and a group of Type III's. In this case, the group of Type III's is really only one Type III, as can be seen at around 60 MHz. Again, non-solar interference from channel 4 is seen at 66 and 67 MHz.

Figure 22 is again a Type V with a group of Type III's. In this example, the observer can see that the burst is visible through the channel 4 interference in the 64 - 72 MHz region.

Figure 23 shows a Type V and a detached Type III. This is a rare burst signature since Type III's are seldom resolved with the 1-sec sweep rate of the SFIR. This burst would start at 1207 UT and end at 1208.9 UT. Although the Type III is detached, it is still reported as a Type V and a group of Type III's.

Figure 24 shows a single Type III at 1147 UT and a group of Type III's from 1205 to 1207 UT. Figure 24 is a good illustration of the difference between a "sharp" and "fuzzy" Type III. The observer should keep in mind that Type III's tend to be "fuzzy" early in the observing day due to ionospheric effects. This ionospheric heating does not happen at corresponding elevation angles in the evening.

Figure 25 shows three groups of Type III's of widely differing intensities. At 1657.2 UT, a well-defined group occurs. At 1641 UT, a less well-defined group occurs, while at 1653.5 UT a very poorly-defined group is observed. The observer is cautioned that these three groups of Type III's do not necessarily correspond to the three intensity classifications. Intensity level can only be determined objectively from the deflection on the total power channel.

Figure 26 illustrates a series of Type III's which turn into a continuum (code 8) at 1635.4 UT. Remember that a continuum contains Type III-like bursts. Some scientists think continua are composed of very closely-spaced Type III's. The key to resolving this ambiguity is twofold.

(a) Does the total power channel return to zero deflection or is it constantly elevated even a fraction of a chart division? If so, a continuum or Type IV is in progress,

(b) Is a noise storm occurring on the 245 MHz discrete frequency radiometer? If yes, you again increase the likelihood of a continuum.

Figure 27 illustrates a Type IV. It is differentiated from the code 8 continuum in the following way:

(a) The total power showed a smooth constant deflection, never, even momentarily, returning to zero deflection,

(b) A flare was observed at 1232 UT giving this burst a flare correlation as mentioned in step "O" of the logic scheme,

(c) The fringe pattern shows no superimposed Type III's imbedded in the continuum. The observer will notice a group of Type III's from 1334 to 1334.7 UT as well as several other groups. These groups are not part of the Type IV because they are "off-fringe". This means the fringe pattern is slightly displaced from the Type IV's fringe. From Section 2, you know this means they are occurring at a physically different point on the sun and are therefore not associated with the Type IV. Recognizing off fringe signatures is a very reliable method of isolating bursts from background continuum.

The slight jogs in the fringe shift that occur near 1334 and 1351 UT are also due to ionospheric effects.

Figure 28 illustrates a Type II. Here a detailed explanation is in order. At 1153 UT the II starts. This part of the Type II extends from 50 to 25 MHz and is the fundamental. At 1155 UT at 75 MHz, the 2nd harmonic begins. At 1157.5 UT, the second band of the 2nd harmonic begins. Remember that Type II's will normally show at least two separate signatures. The burst depicted in Figure 28 is only one Type II. Note several details contained in Figure 28:

- (a) The split banding and harmonic just mentioned,
- (b) The association with a large solar event. (This burst was associated with a centimeter burst as well as a 2B flare),
- (c) The fairly clear-cut start or leading edge of the signature,
- (d) The slope of the leading edge which exhibits the "slow drift" nature of a Type II. The burst begins at 1155 UT at 75 MHz. At 35 MHz, the start of the 2nd harmonic is 1202.2 UT. This is 40 MHz of drift in 7.2 min or about 5 MHz per minute. This is a typical Type II drift rate,
- (e) Also notice the gradual loss of intensity at the end of the burst. This is not a necessary feature of a Type II.

Figure 29 illustrates a Type IV commencing at 1222.6 UT and ending at 1233 UT. This burst was associated with a major flare and centimeter burst. Several details should be noted in this figure:

- (a) The kink in the Type IV fringe pattern at 1230.6 UT is due to the source of the Type IV moving on the sun. Type IV's of this variety are called "moving center" IV's by the scientific community.
- (b) The start of the IV is gradual, beginning at 1222.6 UT with full intensity achieved at 1223.6 UT. This can be contrasted with the groups of Type III's also in Figure 29 at 1237.3 UT that "turn on" in less than 0.1 minutes,
- (c) A continuum was carried simultaneously with this IV and can be seen clearly after 1245 UT.

Figure 30 illustrates a Type V and group of III's as well as TV channel 2 turning on at 1800.5 UT. Channel 4 was transmitting for the entire period. The fringe shift of the V is clearly contrasted with the channel 2 signal in this example.

Figure 31 illustrates a Type V and a group of Type III's.

Figures 32, 33, and 34 are all examples of groups of Type III's with and without Type V's. Figure 32 shows the III's starting at 1506.3 UT and the V at 1507.7 UT. Figure 33 shows a group of III's. Notice the difference in the end of Figures 32 and 33. Figure 32 looks like a flag with twice the duration at 30 MHz as at 60 MHz. In Figure 33, the back side of the group of III's at 1522.7 UT is as abrupt and straight as the start. This is the best distinction between a group of III's with and without a Type V. Figure 34 illustrates a group of Type III's between 1835 UT and 1836.6 UT, a group of Type III's between 1835 UT and 1836.6 UT, a group of III's with a V between 1840.7 UT and 1846 UT, and another group of III's with a V following. In reporting, this entire example could be reported as a group of III's and a V.

Figure 35 illustrates a Type V with a group of III's where the trailing edge or burst end is straight and could be confused with a simple group of III's. The deciding factor which clearly categorizes the event as containing a Type V is the abruptness of the end. In this case, the burst ends at 1307.4 UT in a much less abrupt manner than the pair of Type III's ending at 1258.3 UT.

Figure 36 illustrates an ambiguous burst. Even an experienced observer or scientist would be unable to tell whether Figure 36 illustrates a Type IV or a continuum without some additional information. The key to the identification is whether it is coincident with a significant flare or centimeter radio burst. The 2N flare associated with this burst confirms a Type IV.

Figure 37 illustrates a clear cut Type IV. Although a Type III burst occurs at 1521.7 UT, it shows fringe shifting; therefore the smooth unstructured burst that is left must be a Type IV. In this case, if no flare or centimeter burst is observed, the associated major event was probably behind the solar limb. The observation of a Type IV may be the only indication of a proton flare beyond the limb. SFIR observations can indicate activity up to two days before a coronagraph. This is particularly important for west limb flare sites that may produce protons at the earth.

Figure 38, a normal code 8 continuum should be viewed in contrast to Figure 37. Figure 38 shows the classic "bursty" structure of a dekameter continuum. It occurred in coincidence with a 245-MHz discrete frequency noise storm.

Figure 39 illustrates a Group of III's and a V followed at 1926.4 UT by a Type IV. At 1931.4 UT, the burst ends abruptly due to the paper being advanced. Advancing the paper to preview a burst on an electrostatic copier will degrade the data record.

Figures 40, 41, and 42 illustrate Type II bursts in conjunction with III's and continua. In Figure 40, the Type II is between 1956 UT and 2002 UT.

Figure 41 is a Type II with a Type V and a group of Type III's, and shows a Type II whose start is simultaneous with a Type III and V. Figure 42 was extremely difficult to analyze in real-time and only the harmonic and major burst coincidence hinted at its Type II character.

Figure 43 illustrates the real data record corresponding to the classical major event schematically illustrated in Figure 44:

- (a) At 1353.2 UT, a group of III's and V in excess of 1 million solar flux units occurred in coincidence with a 2B white light flare, as well as a discrete frequency burst in the centimeter range. This event produced detectable protons,
- (b) At 1359.5 UT and 1401.2 UT, the fundamental and 2nd harmonic of a Type II are discernable only as fringe shifts. Immediately after the II a Type IV commences and continues until the end of the figure,
- (c) Figures 45 and 46 illustrate groups of III's and strong Type V's.

4.4 Jupiter Bursts

Although this report is intended as a manual on solar burst identification, the SFIR will detect radiation from sources other than the earth and Sun. The planet Jupiter is a radio star, and as such periodically generates dekameter bursts. Figure 47 illustrates a Jupiter burst picked up on the Sagamore Hill SFIR. Jupiter bursts which have been statistically correlated to Jupiter's moon, Io, have three characteristics:

- (a) They always show a frequency cutoff above 40 MHz. No higher frequency Jupiter bursts have ever been observed,
- (b) Jupiter bursts last typically 2 to 5 minutes,
- (c) Jupiter bursts are smooth, featureless, weak bursts with a quick turn-on and turn-off time.

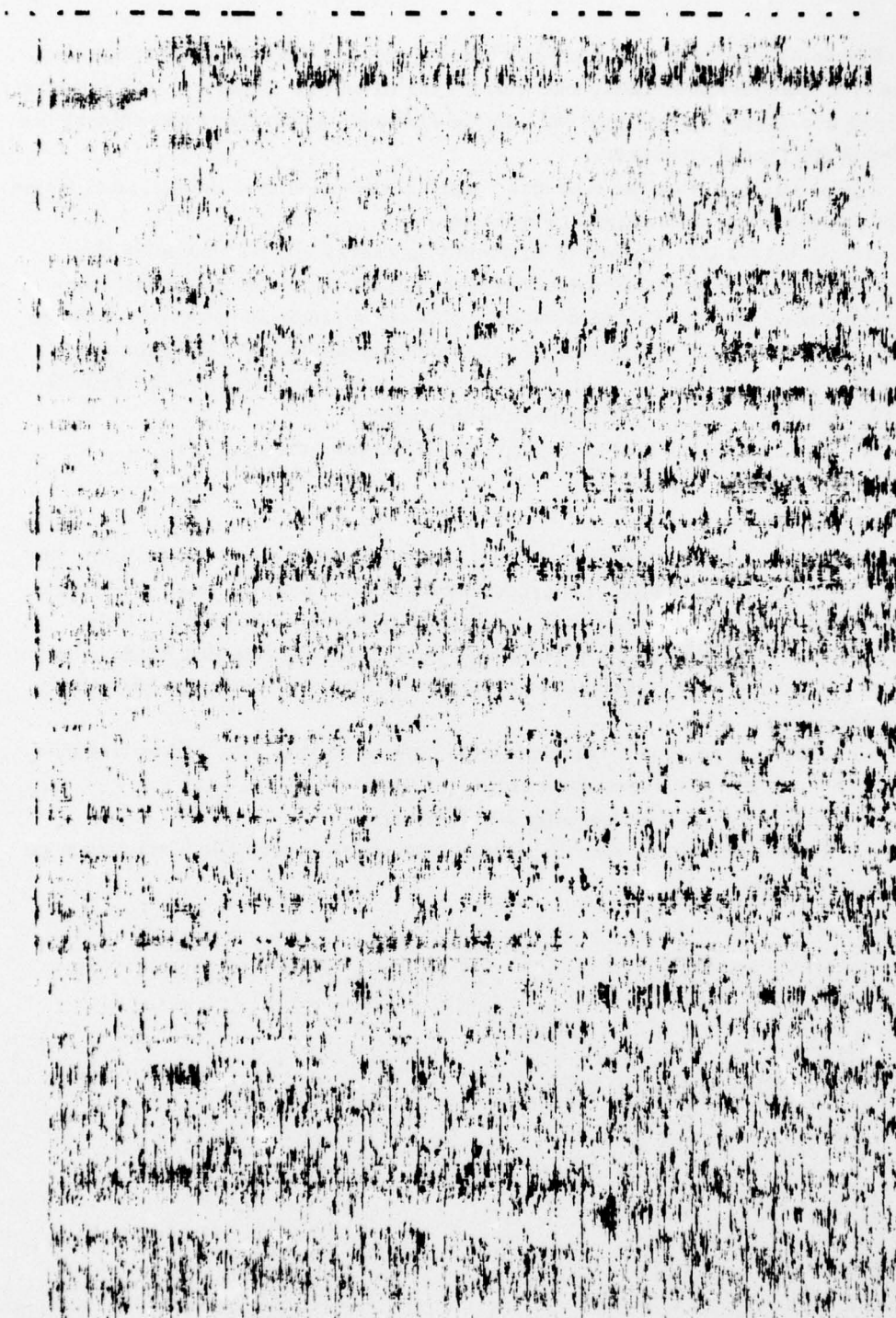


Figure 19. SFIR Data Sample-No Signal

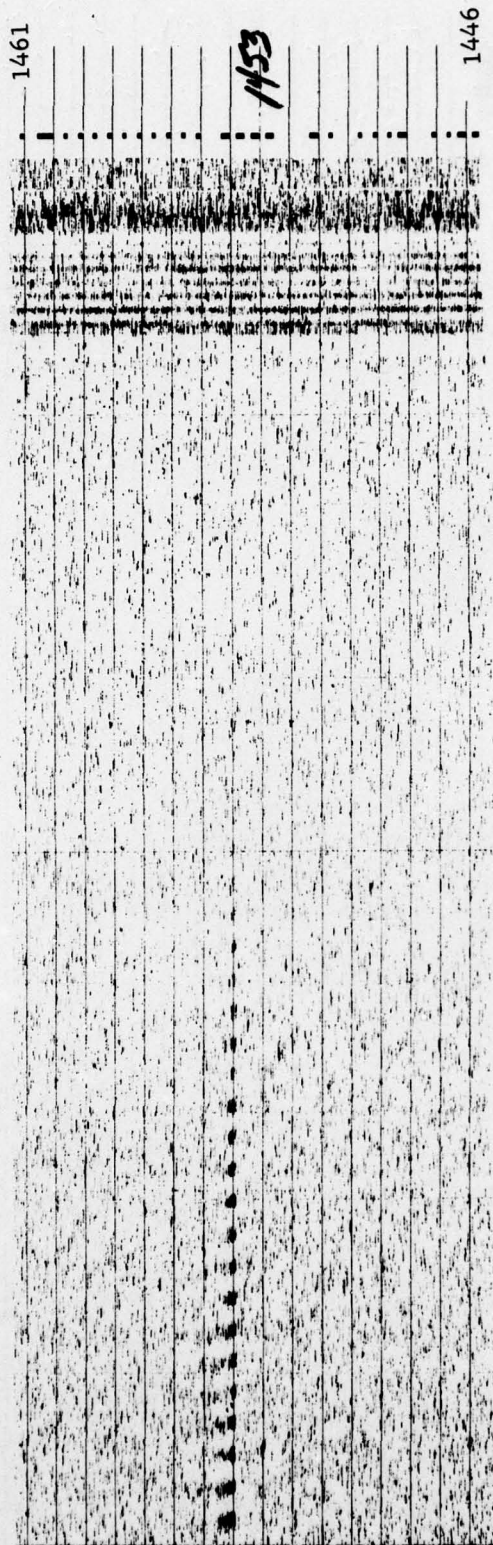


Figure 20. Type V and Type III Solar Radio Burst

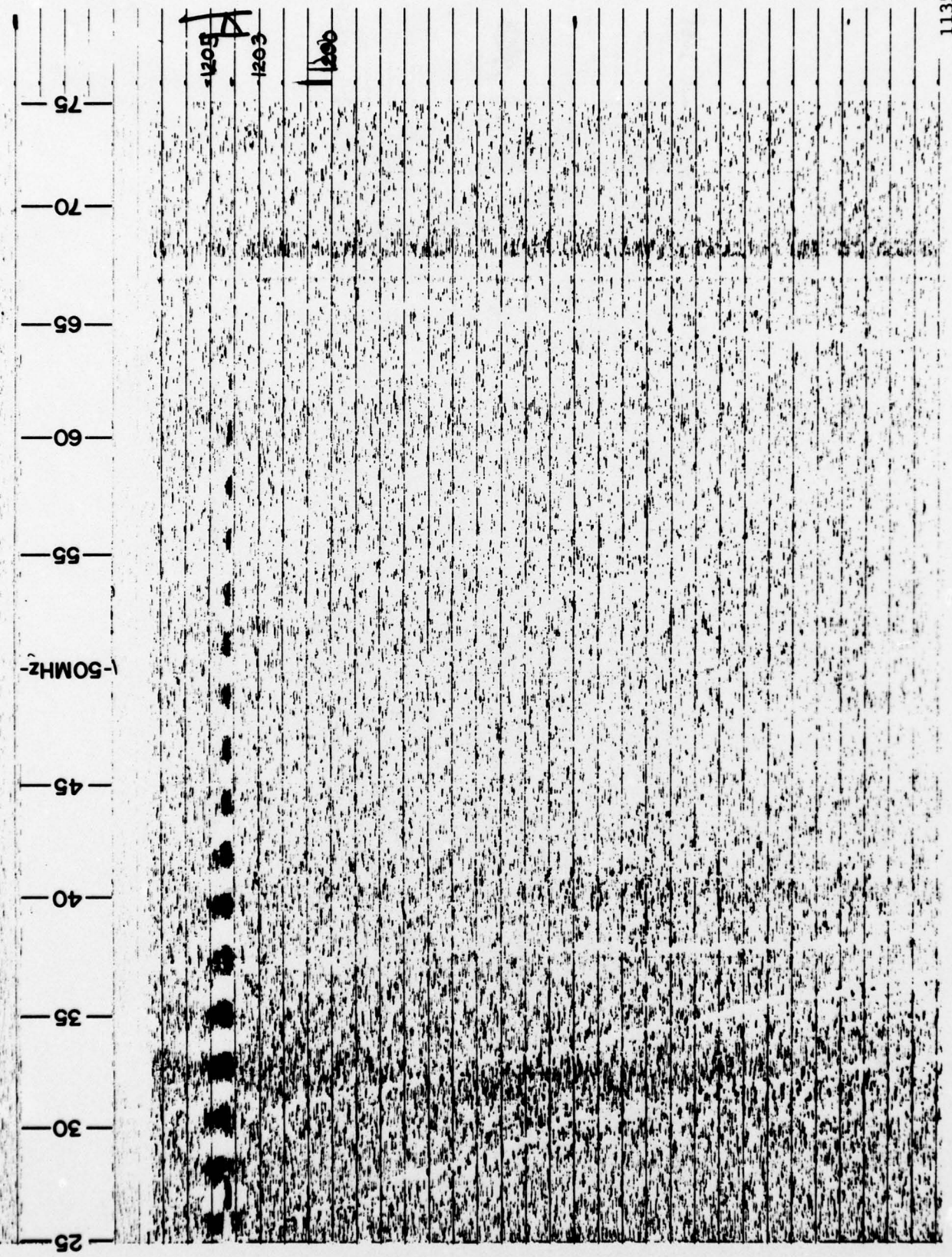


Figure 21. Type III and Type V Burst



Figure 22. Type V and Group of Type III's

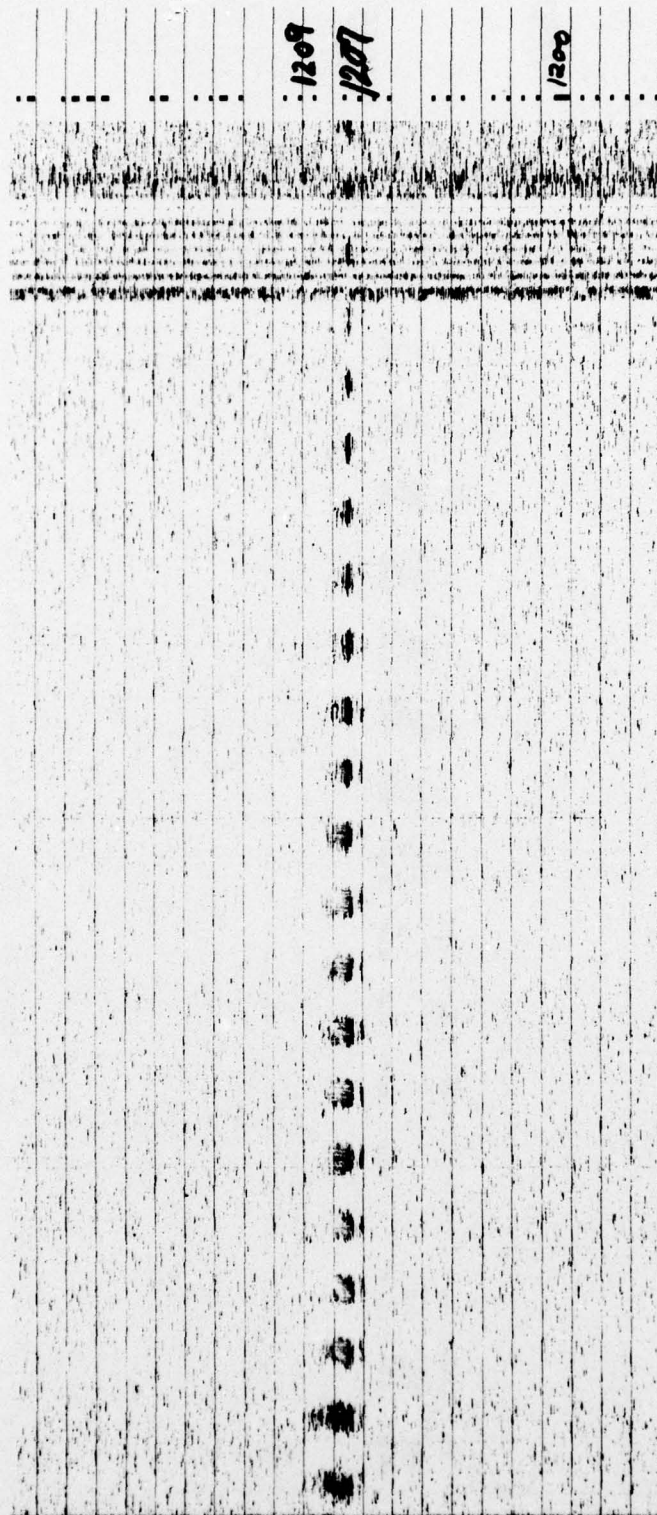


Figure 23. Type V and Detached Type III

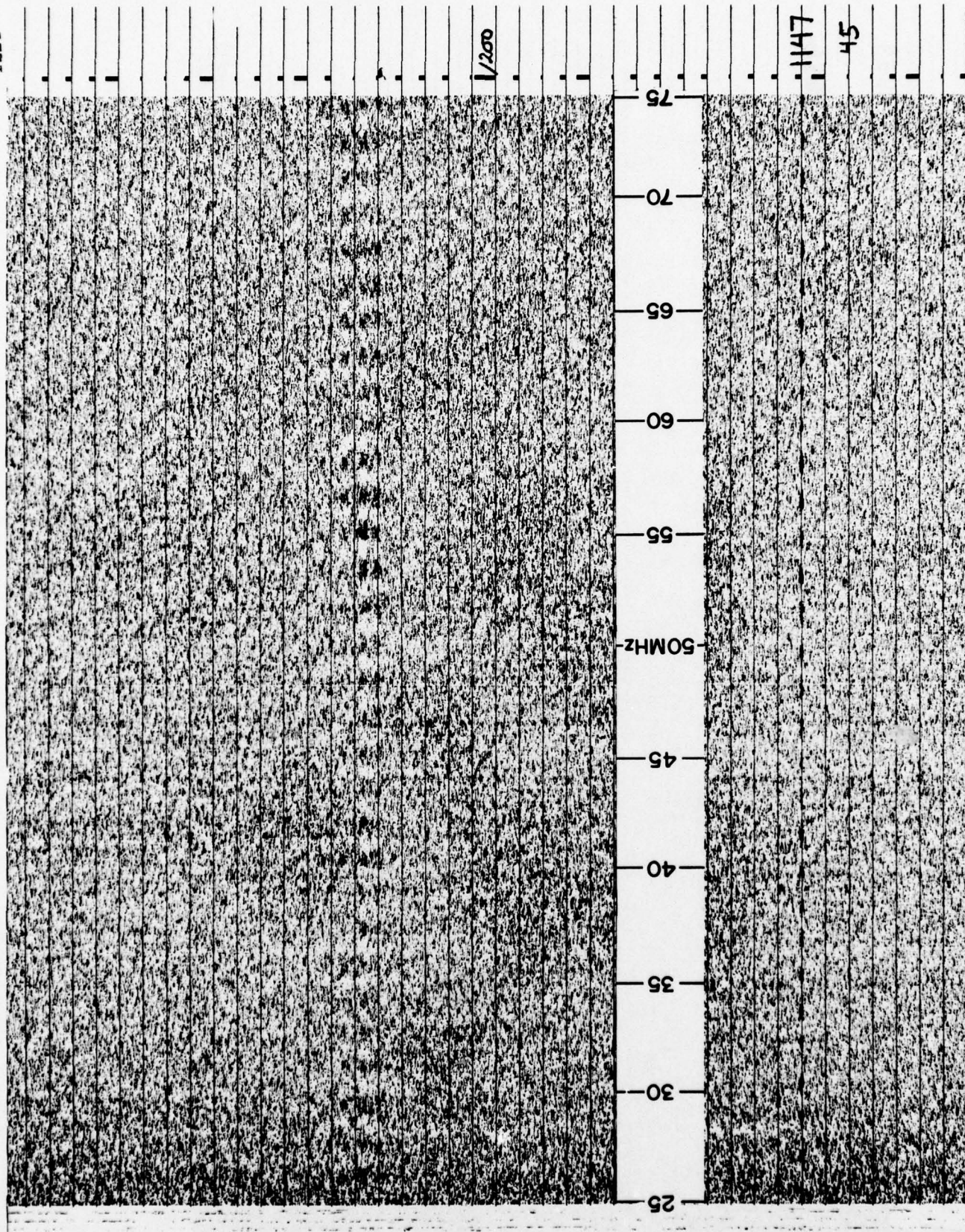


Figure 24. Type III and Group of Type III's

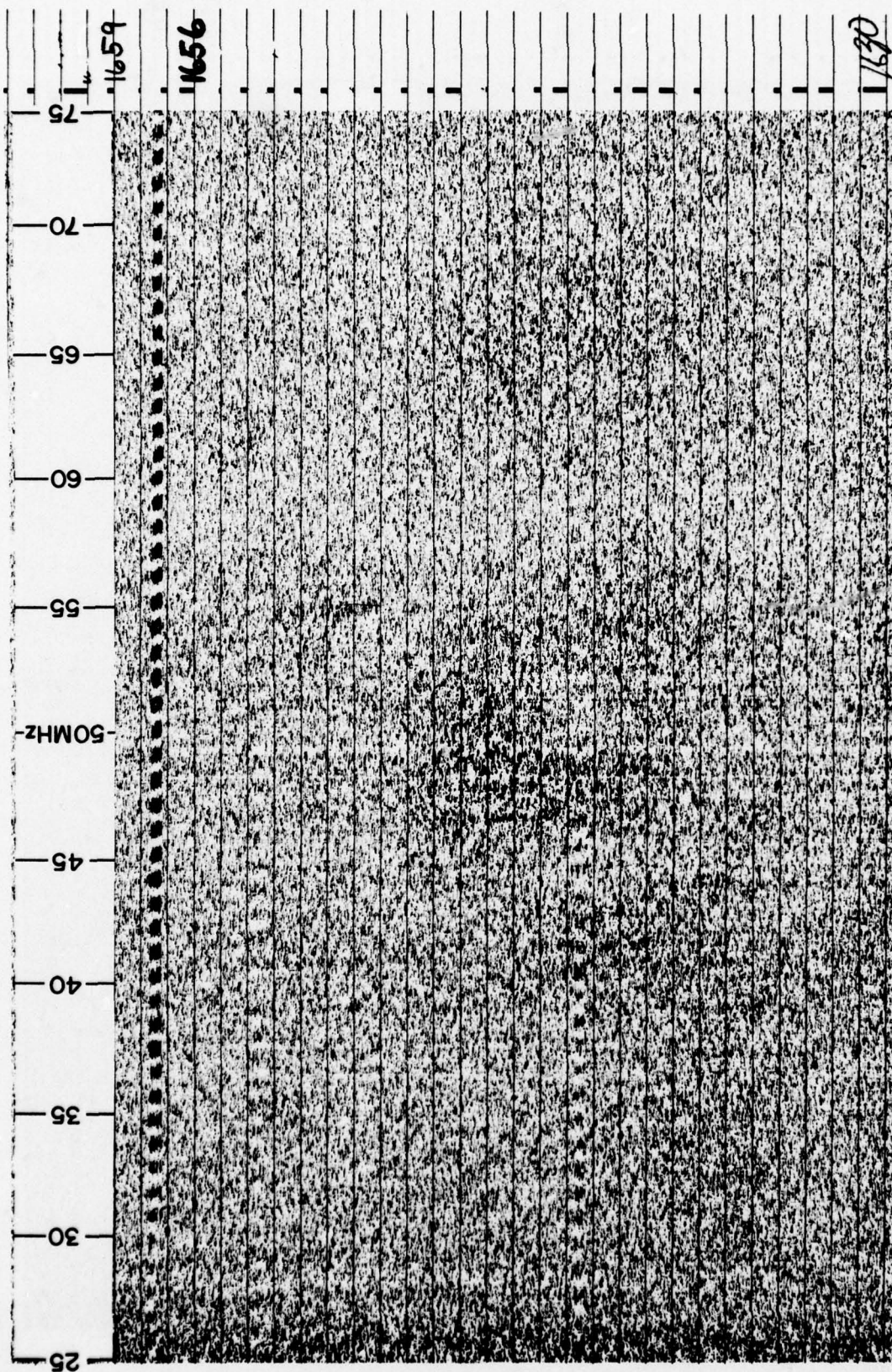


Figure 25. Three Groups of Type III's of Varying Intensities

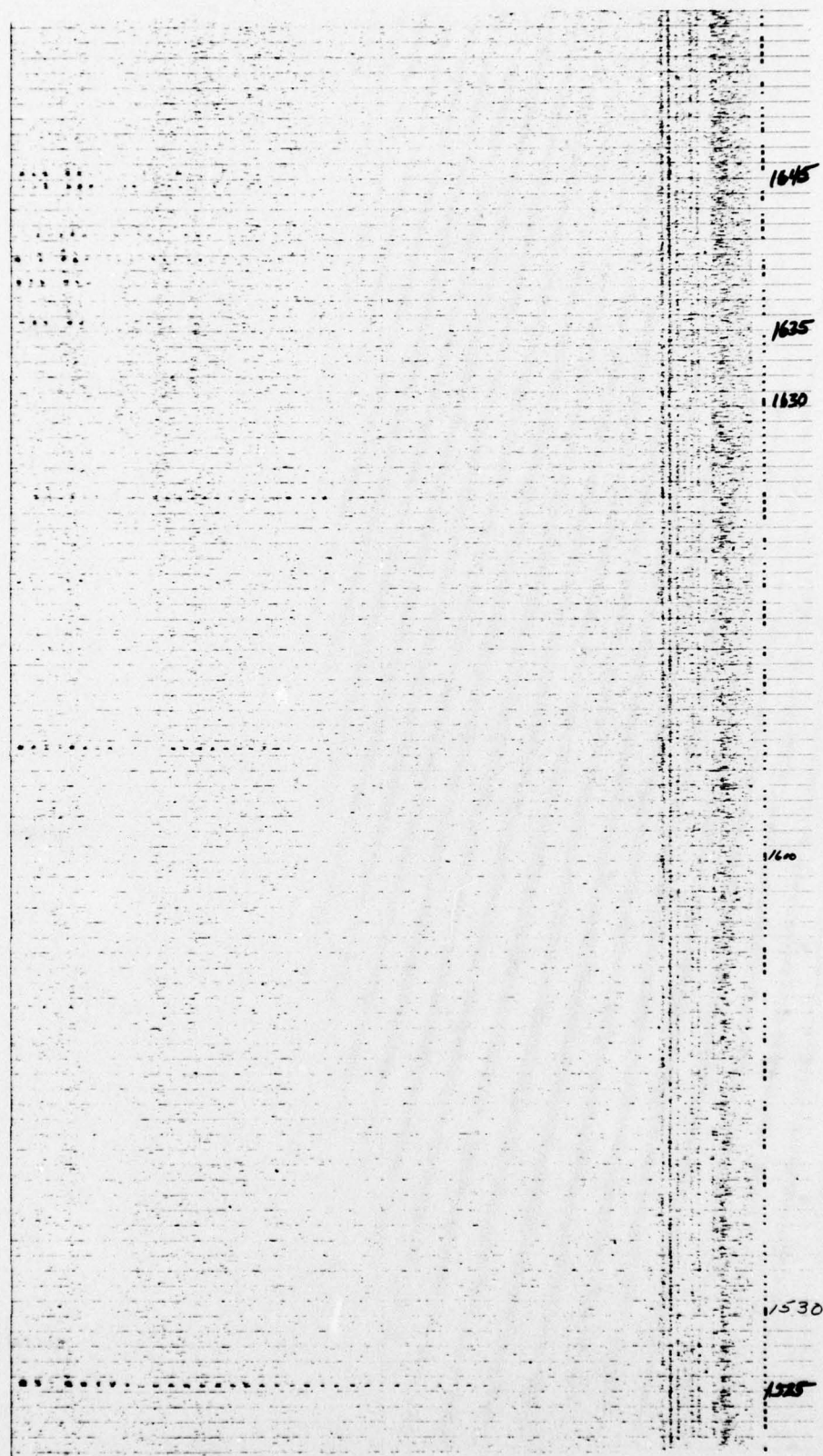


Figure 26. Series of Type III's and Continuum

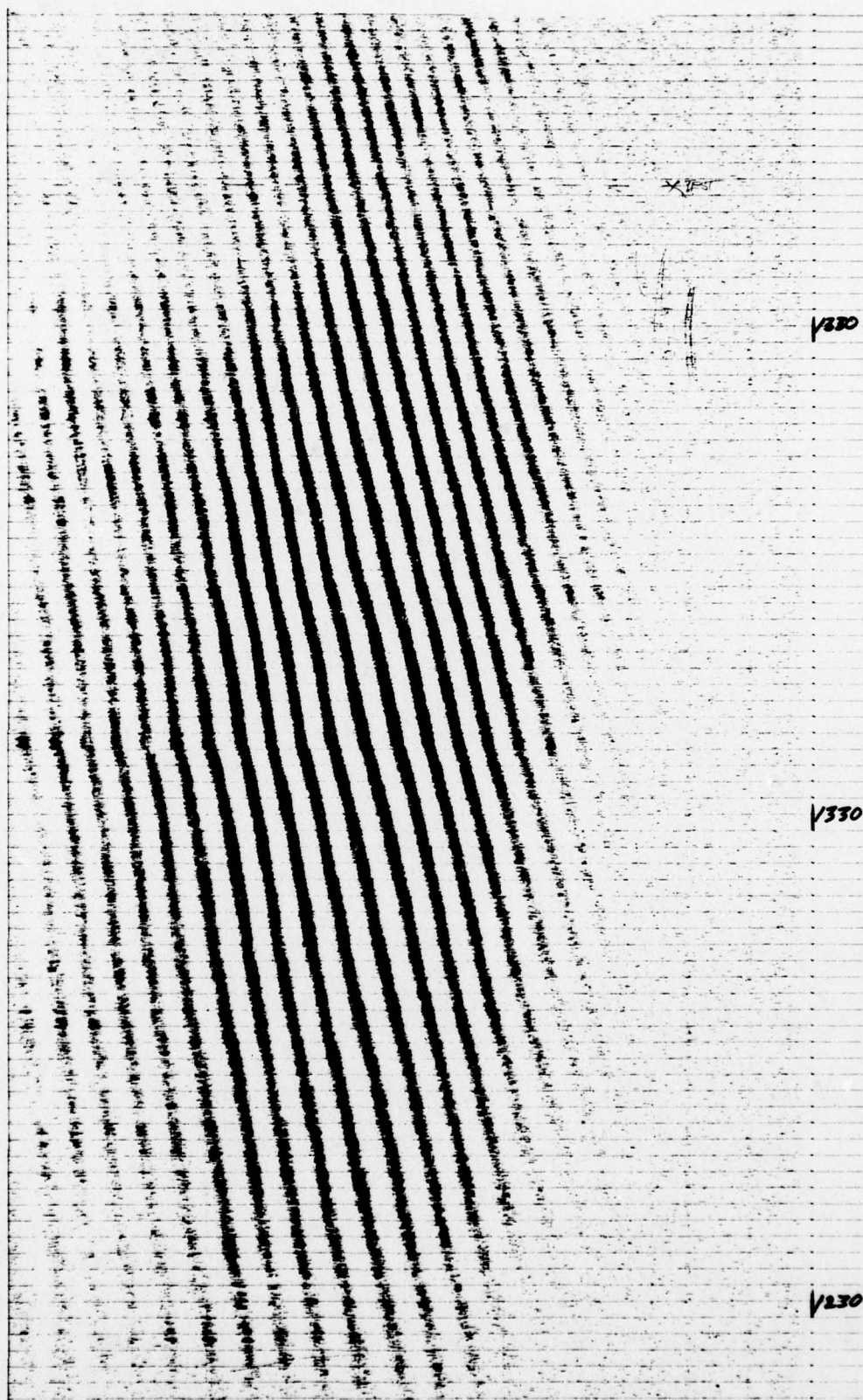


Figure 27. Type IV

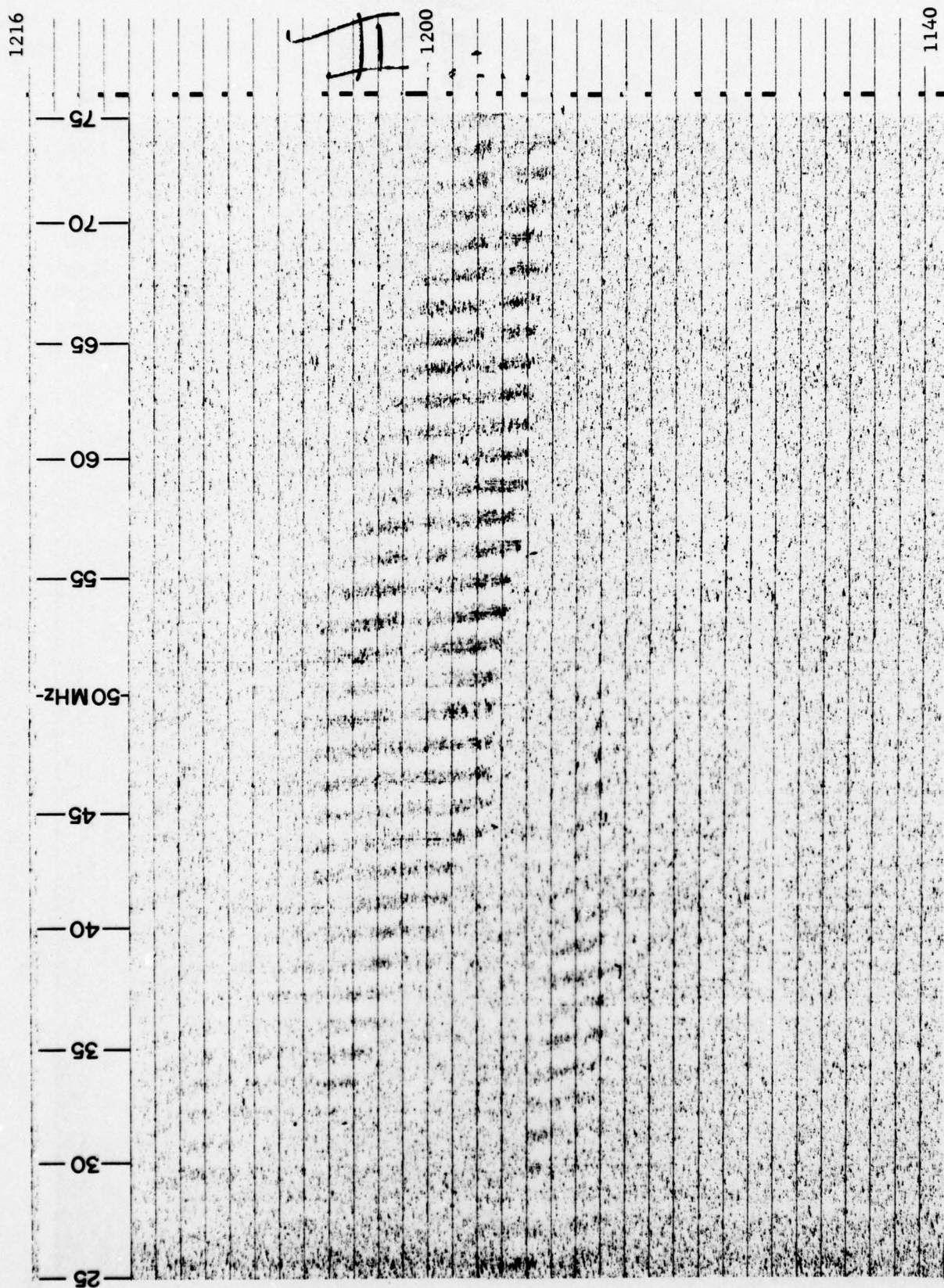


Figure 28. Type II

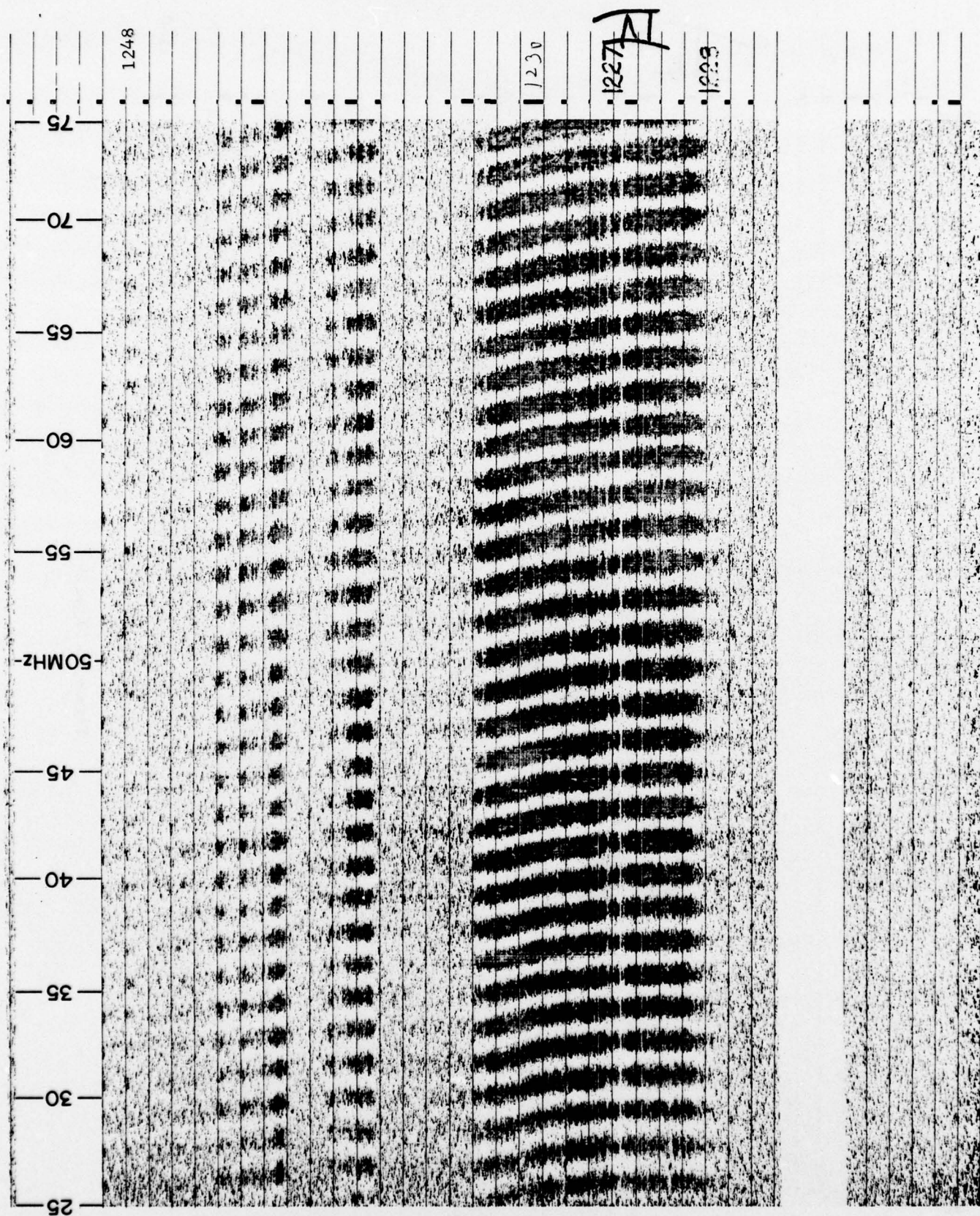


Figure 29. Type IV, Group of Type III's and Continuum

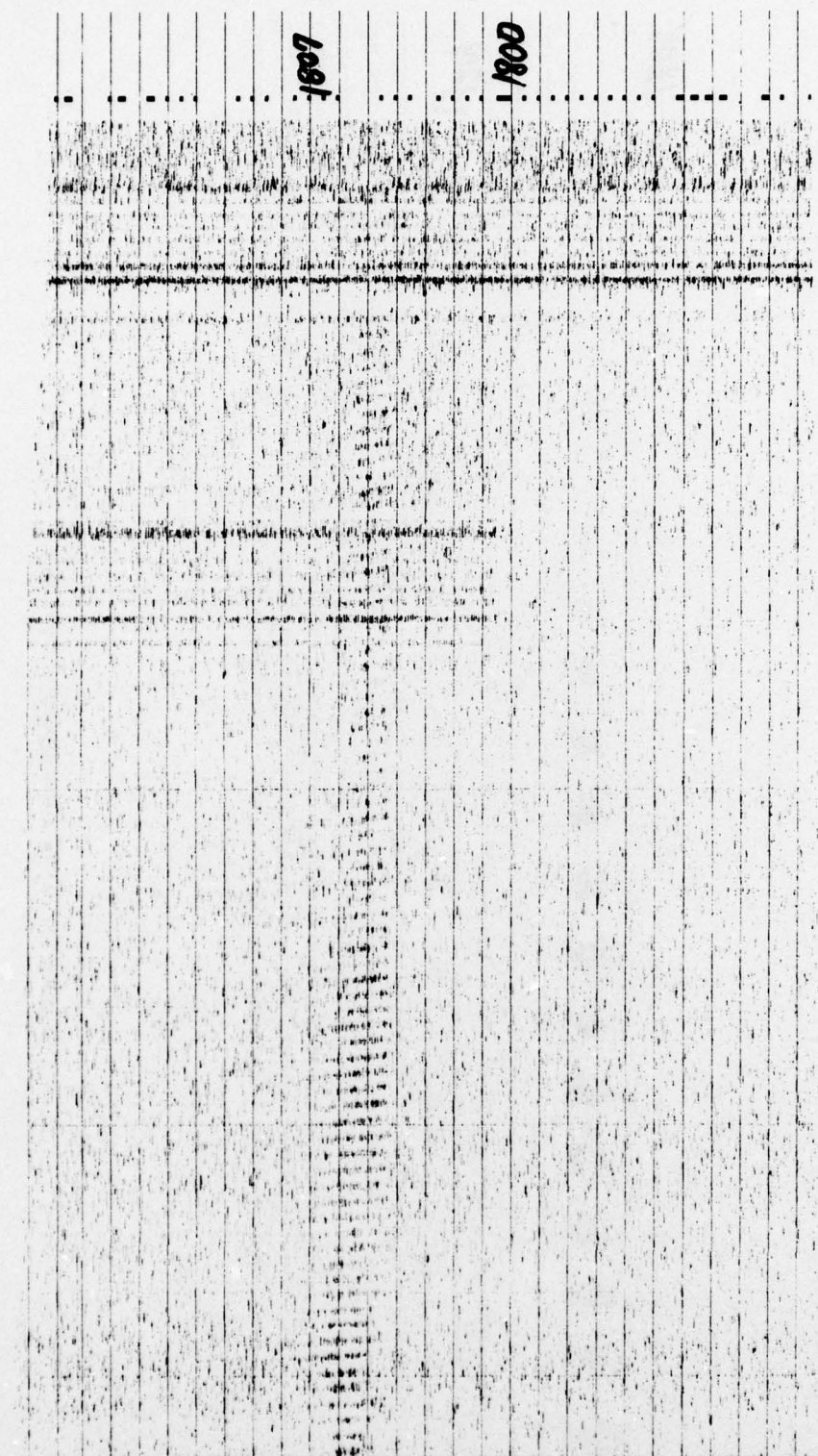


Figure 30. Type V and Group of Type III's Plus TV Channels 4 and 15

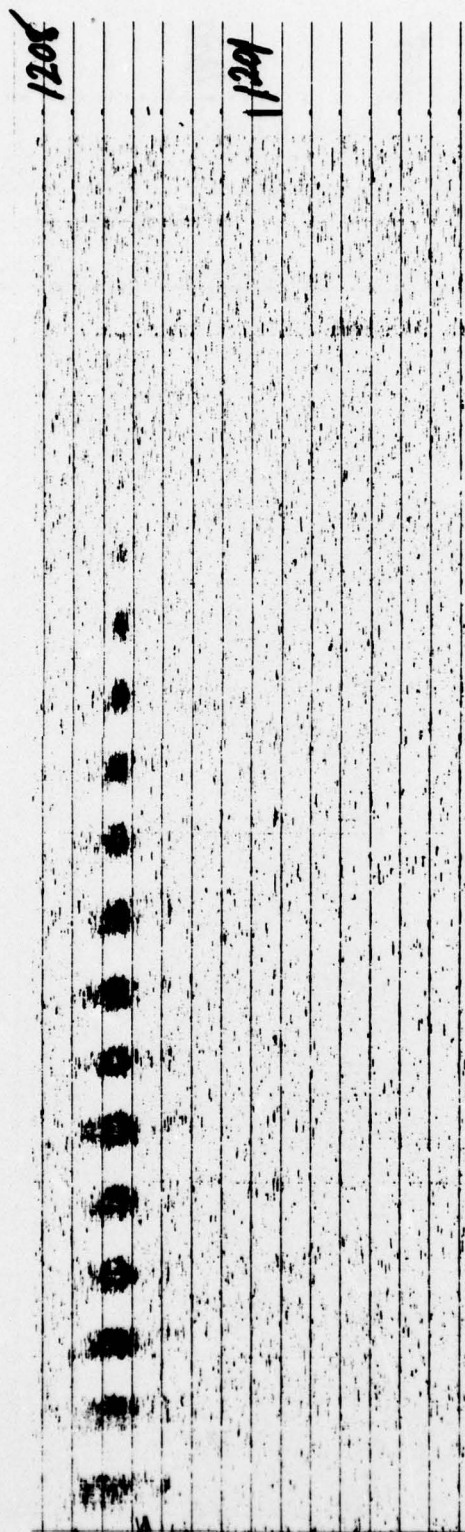


Figure 31. Type V and Group of Type III's

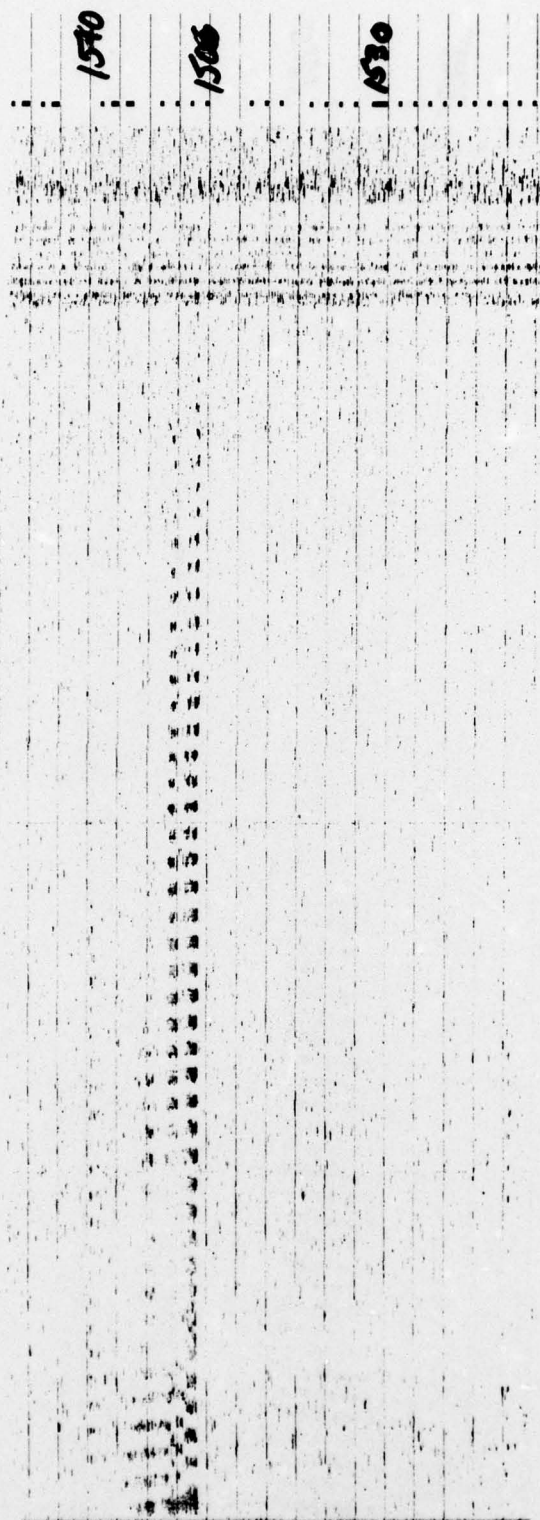
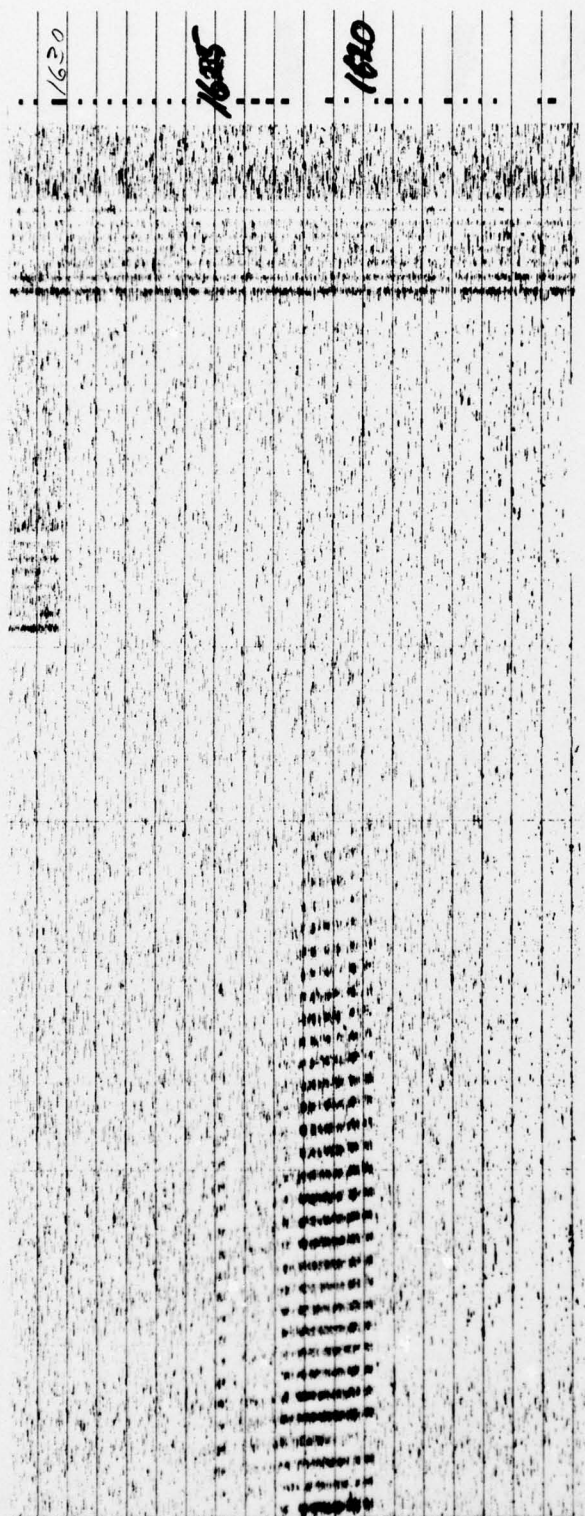


Figure 32. Type V and Group of Type III's



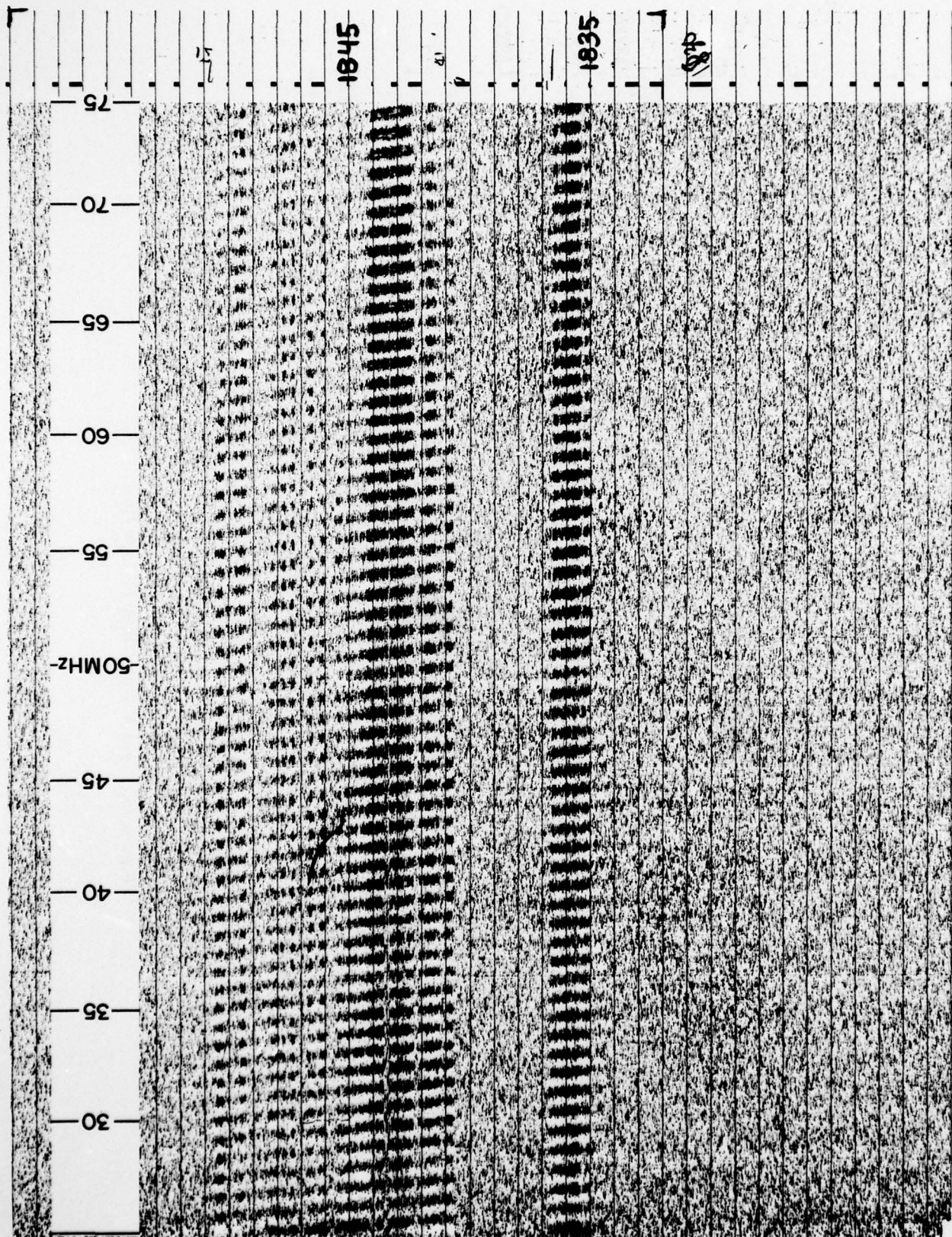


Figure 34. Type V and Group of Type III's

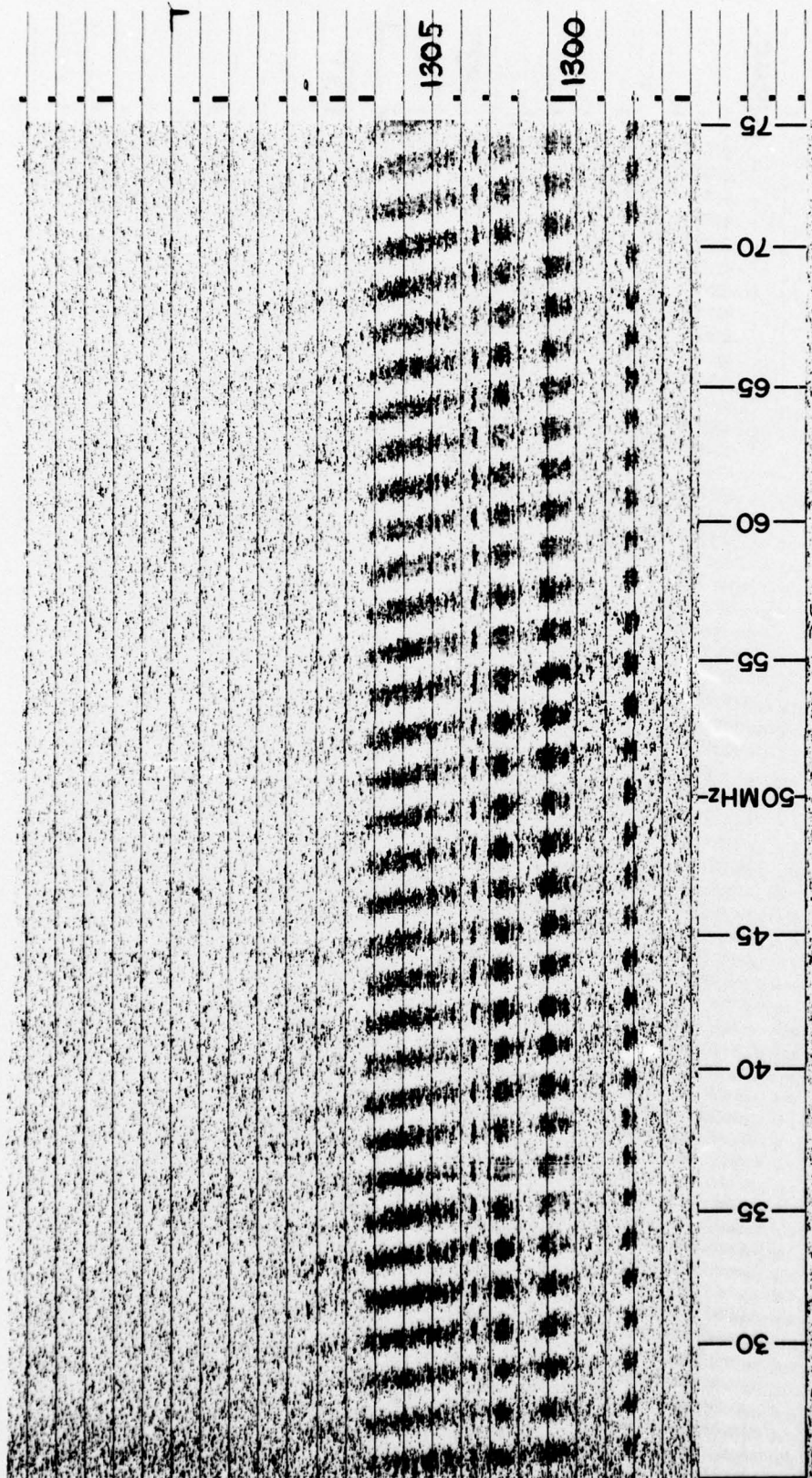


Figure 35. Type V With Group of Type III's

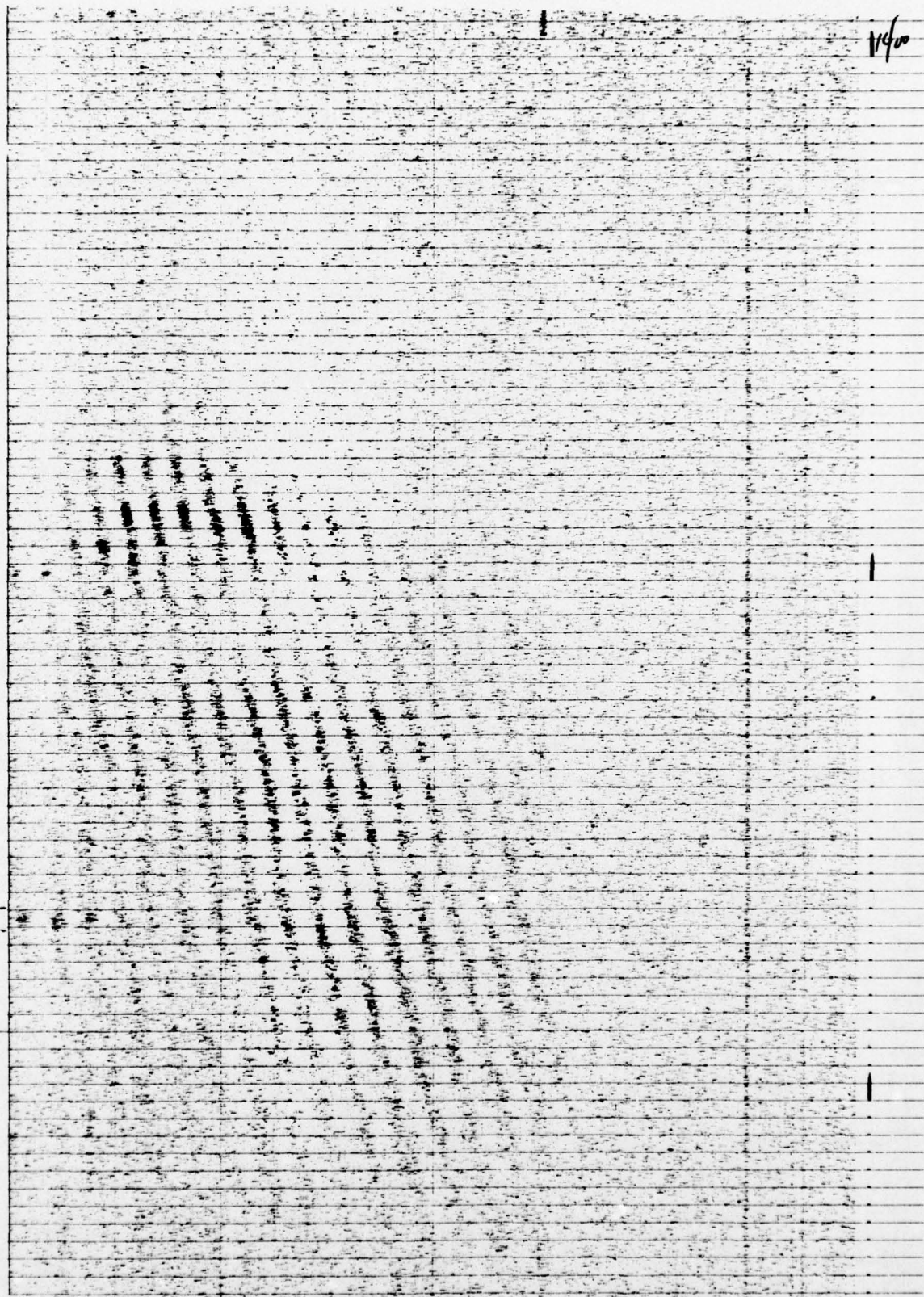


Figure 36. Type IV

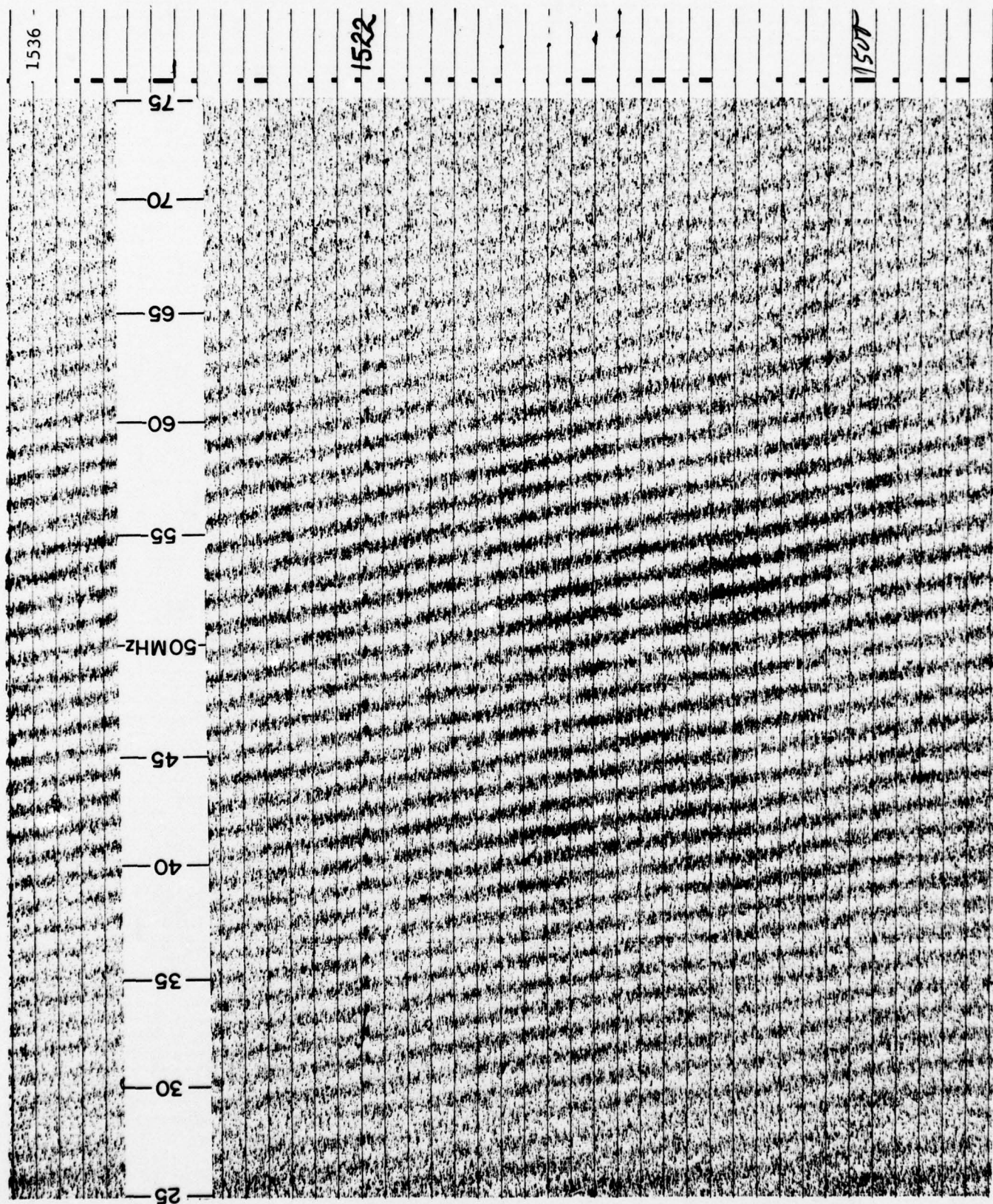


Figure 37. Type IV and "Off Fringe" Type III

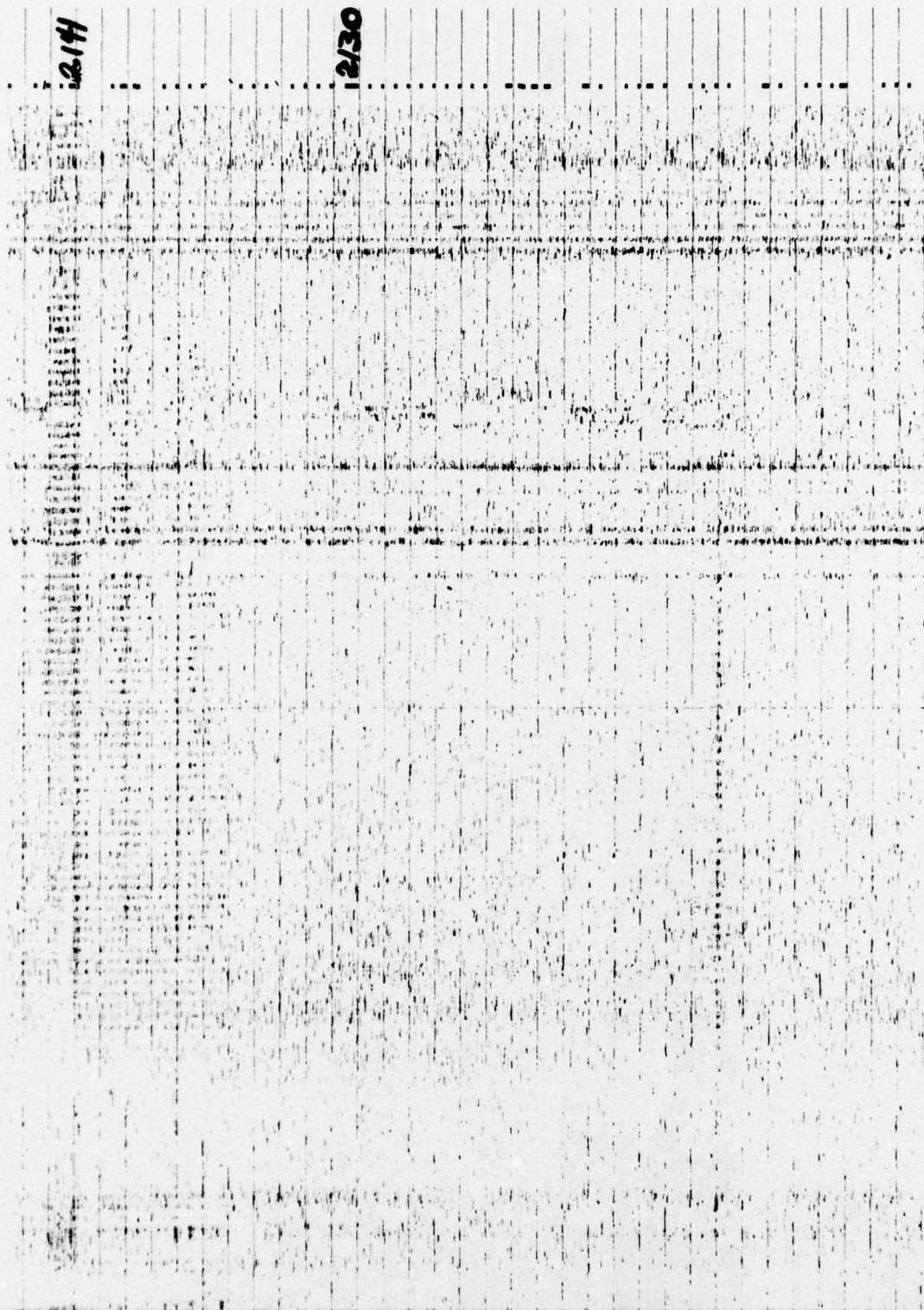


Figure 38. Continuum

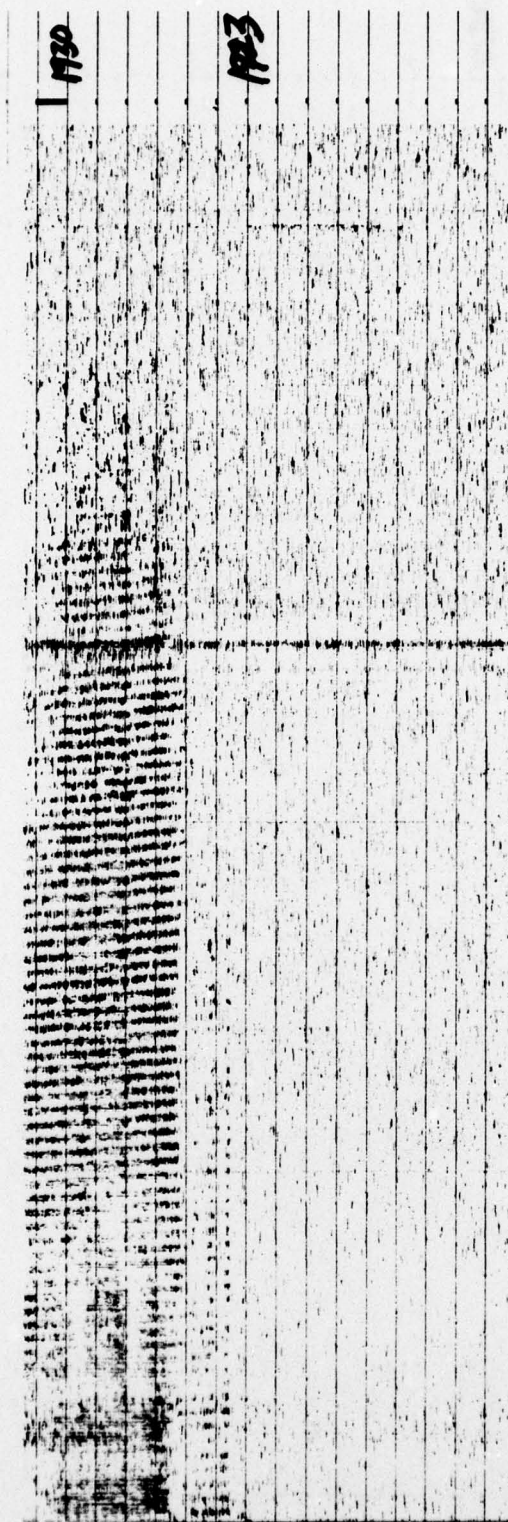


Figure 39. Type V With Group of Type III's

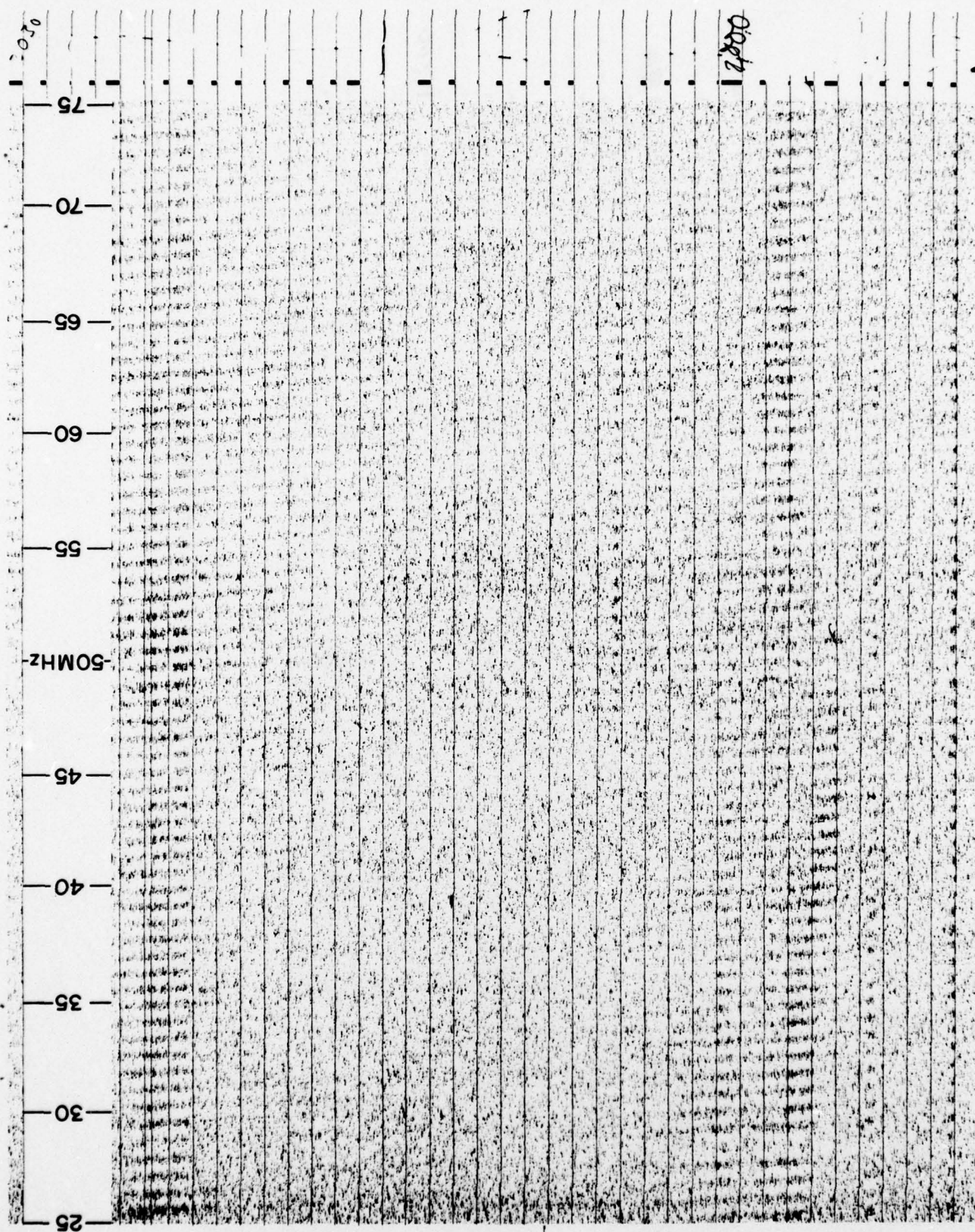


Figure 40. Type II With Group of Type III's

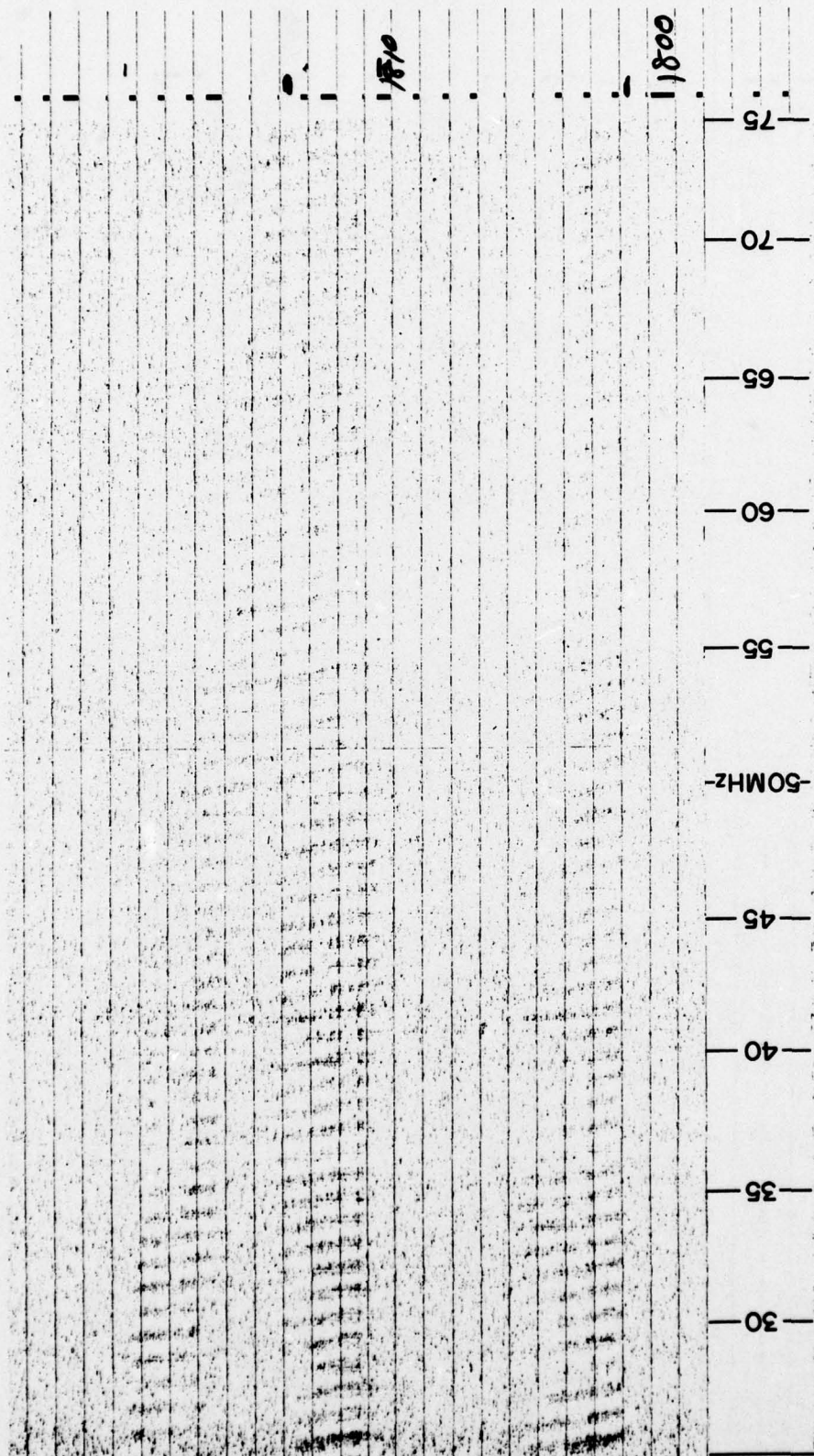


Figure 41. Type II With Type V and Group of Type III's

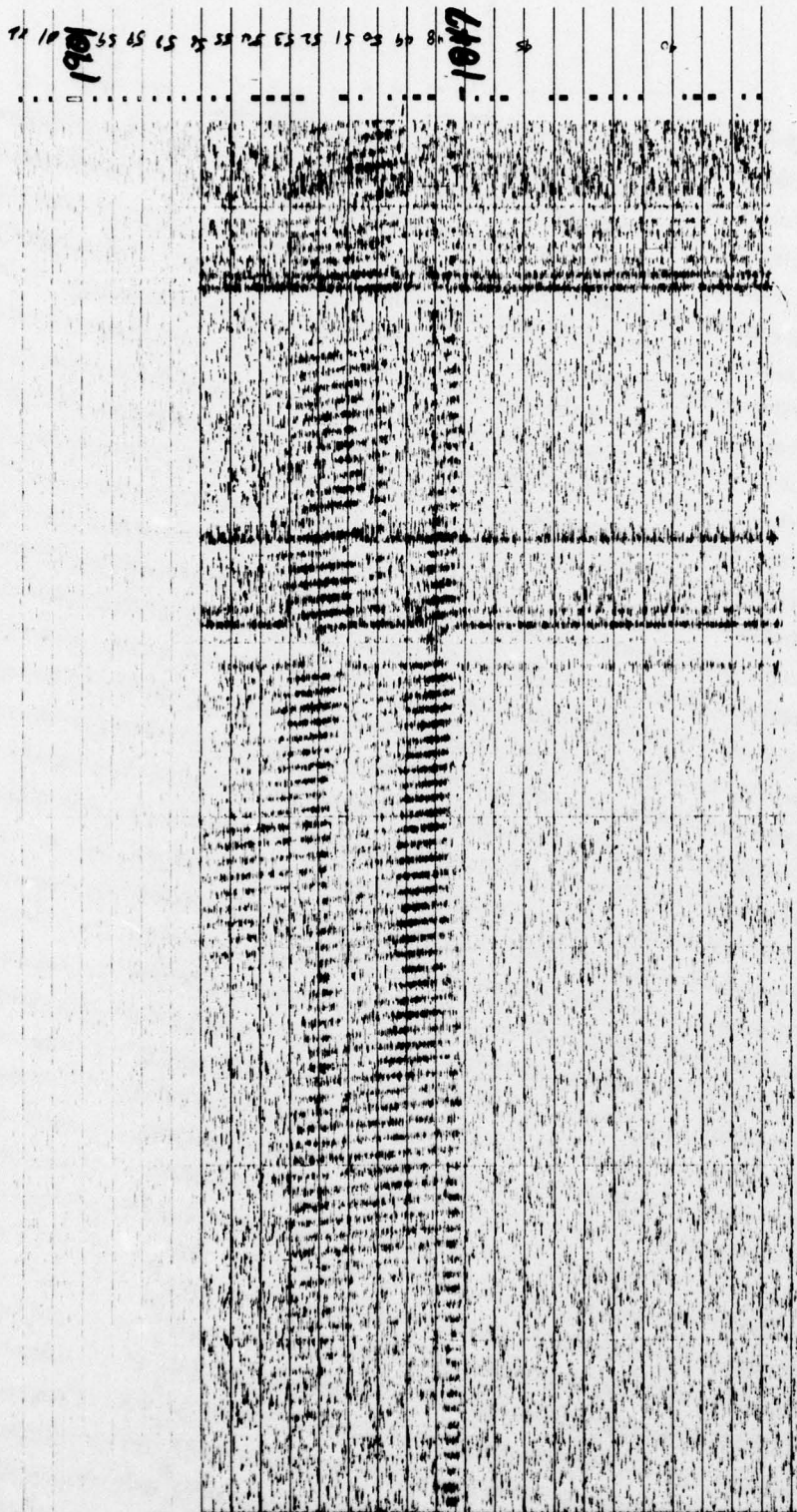


Figure 42. Type II With Type V and Group of Type III's

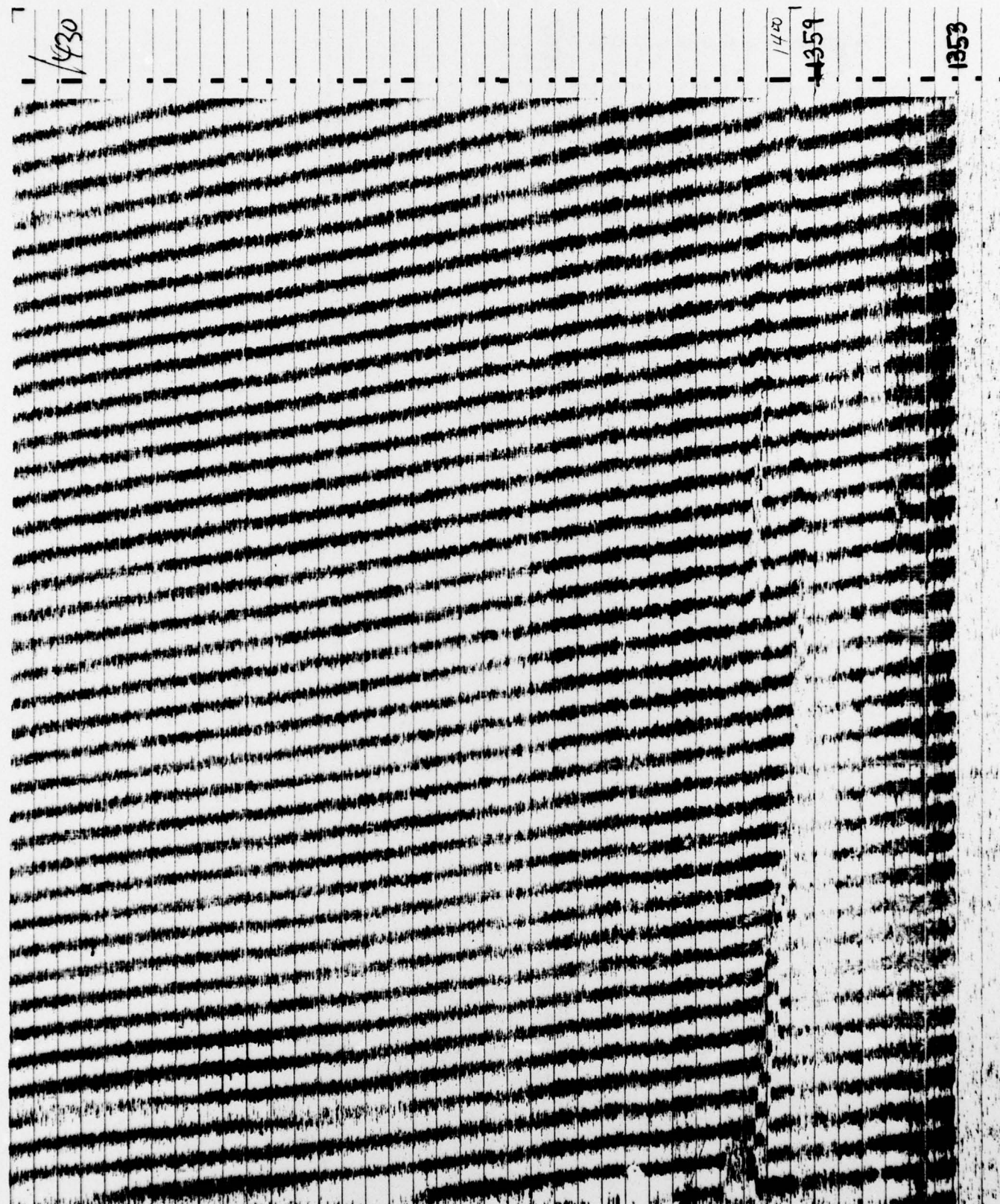


Figure 43. Classical Major Event With Type V and Group of Type III Followed by Type II and Type IV

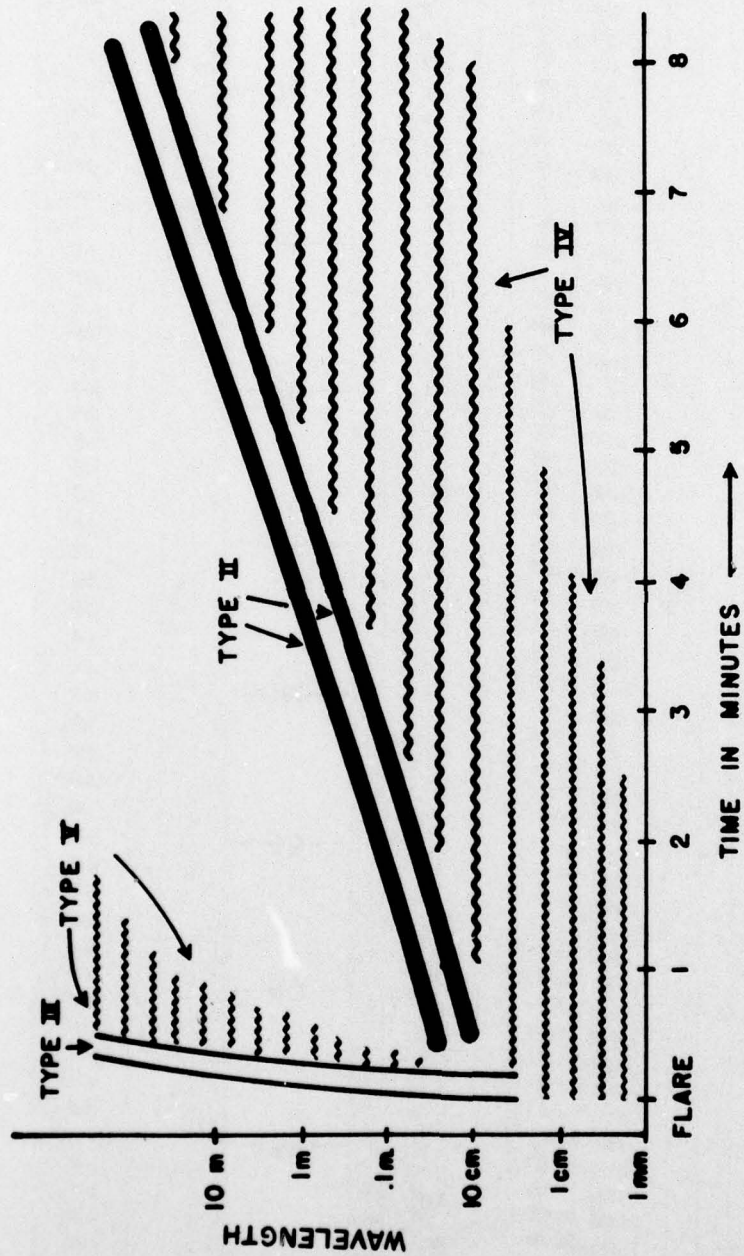


Figure 44. Schematic Representation of Major Event Similar to Figure 38

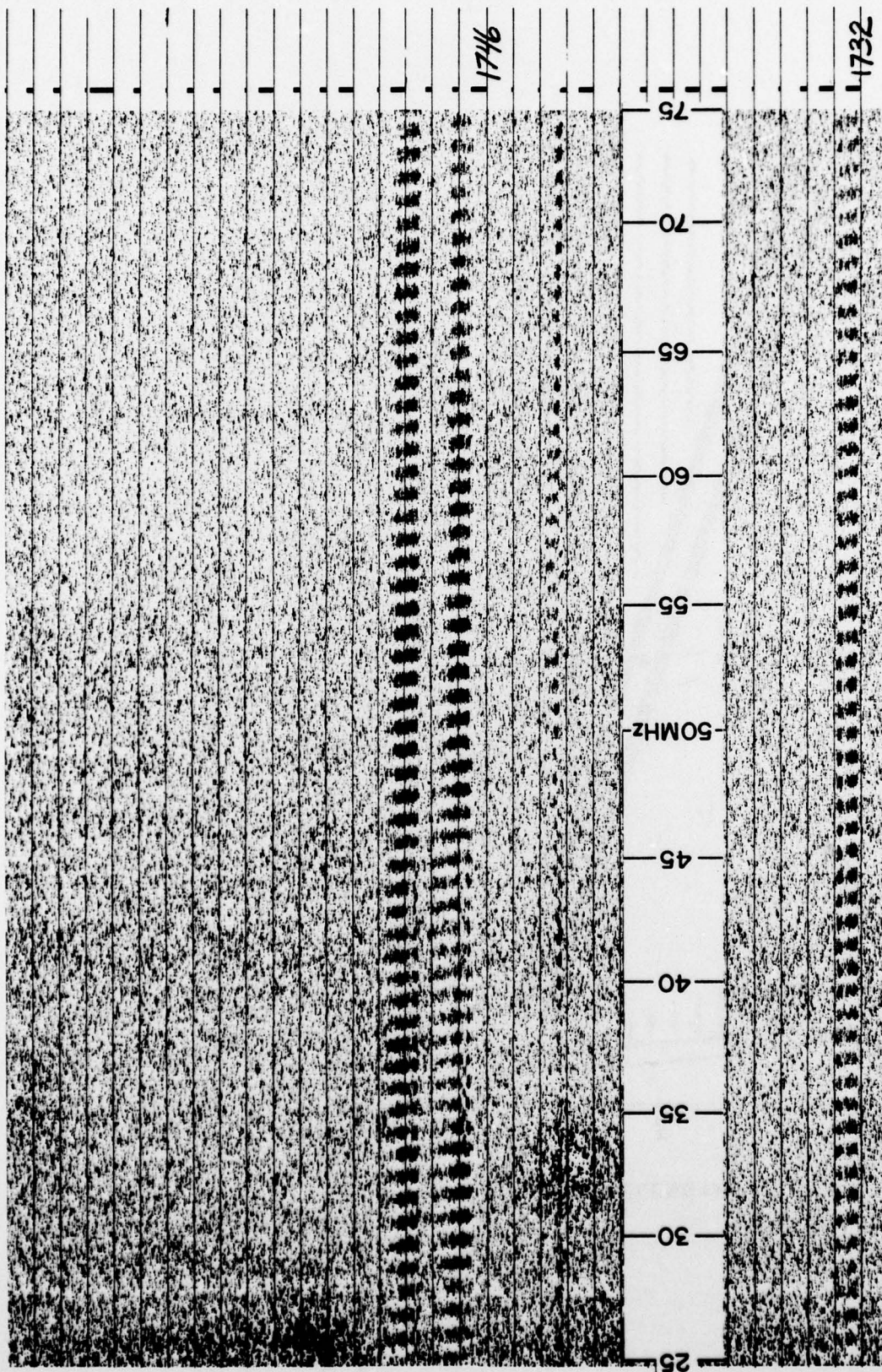


Figure 45. Strong Type V and Group of Type III's

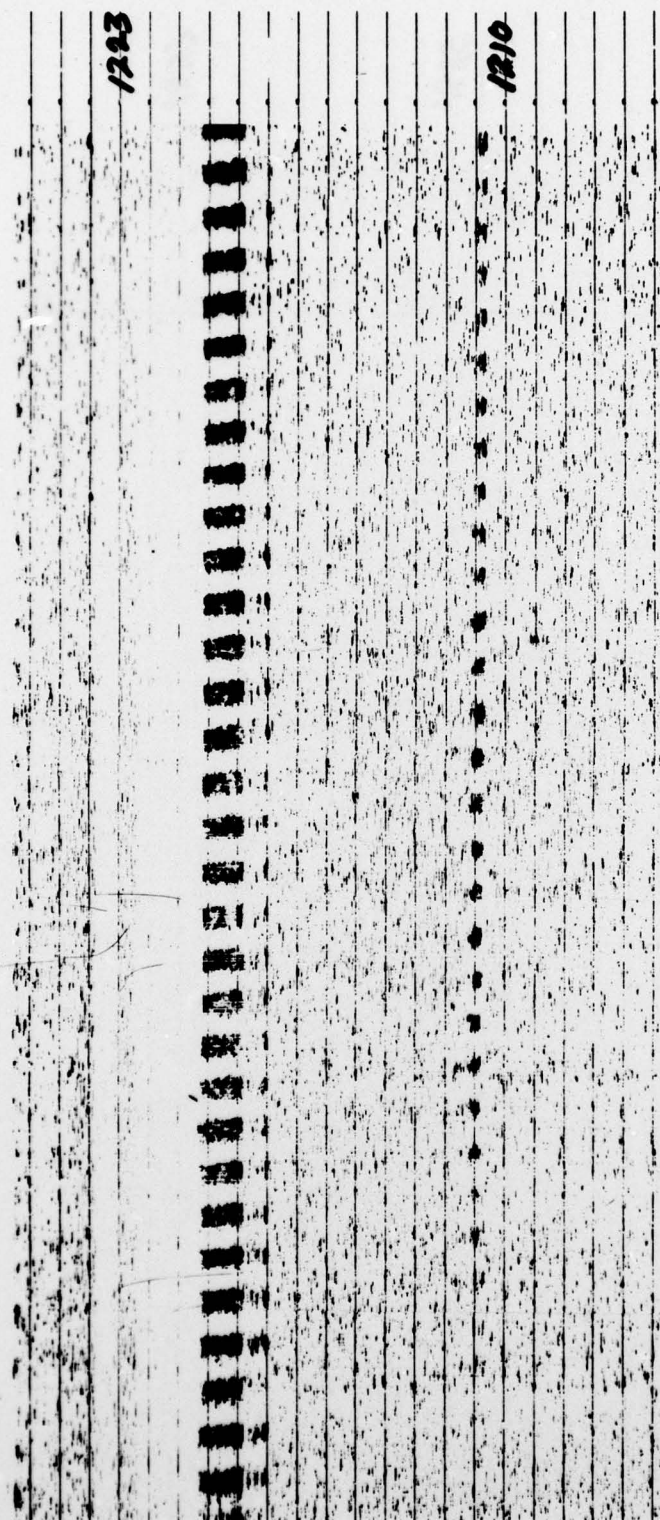


Figure 46. Strong Type V and Group of Type III's



Figure 47. Jupiter Burst

4.5 Burst Classification Hints

Several suggestions can be made that should be in mind when trying to determine a burst classification.

Always remember that the fringes are shifting at a constant rate with time. At Sagamore Hill, the rate is about 7.8 MHz per hour toward the 25-MHz margin. This rate varies as the solar interferometer baseline geometry varies but remains close to the same figure indefinitely. Each observer at each station should become familiar with their SFIR's drift rate. Fringes observed to drift at a much faster or slower rate than this should not be considered solar in origin. Any signal that stays at the same frequency, no drift, (like the TV signals in many of the previous examples) is caused by local interference.

Figures 26 and 27 are also examples of ionospheric effects. Figure 26 shows background intensity fluctuations due to ionospheric effects. From 25 to 40 MHz, broad diffuse lines begin around 1535 UT and continue through the end of the example. These broad lines, which do not drift in time, have only vaguely recognizable fringes. Note that the fringe widths are three to four times as wide as the fringes of solar origin. These broad diffuse non-drifting fringes are actually due to manmade radio traffic reflecting off the ionosphere and into the SFIR's beam pattern. Normally, the ionosphere is so transparent that it does not act as a mirror at all. Another ionospheric effect is illustrated by Figure 27. The slight kinks or bends in the fringe pattern are caused by ionospheric refraction. This effect is observed optically on a hot day when objects on the horizon seem to jump due to the heat waves coming off of the ground. The heat waves are actually density gradients that cause the atmosphere to act like a lens. Density gradients in the ion/electron density of the ionosphere cause the image of the sun to oscillate about its true position. This oscillation appears as interference fringe pattern displacements as in Figure 27. Both types of ionospheric effects are more frequent and more intensive at the low sun angles, local sunrise, and sunset.

Remember that fringes get "fuzzier" as their intensity decreases. This is due to the decreasing signal-to-noise ratio of the entire SFIR system. Figure 24, a group of Type III's at 1205 UT and a single III at 1147 UT, illustrates this effect. The group is fuzzy due to its lower intensity. Figure 36 is even more graphic. This is a weak Type IV. The "intensity" fluctuations were due to the electrostatic printer and not intensification of the sun. If intensification were occurring, the fringes would have become "less fuzzy" and the total power channel would have shown a rise.

"Fuzzy fringes" can also mean a larger source of solar emission. Interferometers sense position, so they also can give an idea of the physical size of the radio-emitting region. If the source is larger than the angular resolution of the

interferometer (see Section 2), the fringes will tend to smear and become wider. Figure 26, the ionospheric fringes are a result of a very large radio source.

The observer will see bursts of weaker intensity if he holds the edge of the data to his eye and sights along the fringes. This allows the eye to integrate more data, effectively improving the signal-to-noise ratio. Very weak bursts will jump out at you, if you practice this technique.

Know what to expect before you look at the record. If the observer knows what the fringe spacing is at the time of the observation, he is less likely to be confused by RFI and more likely to notice faint bursts.

NOTE: The CEC interferometers have an antenna-reversing switch that will reverse the spacing at noon. In this case, the fringe spacing increases after the switch is activated.

4.6 Observational Hints

Know what to expect from the sun. Figure 48 illustrates an active region producing dekameter bursts as it is rotating into view with respect to the earth. A large flare-producing active region will produce observable emissions as it rotates into view in the following order.

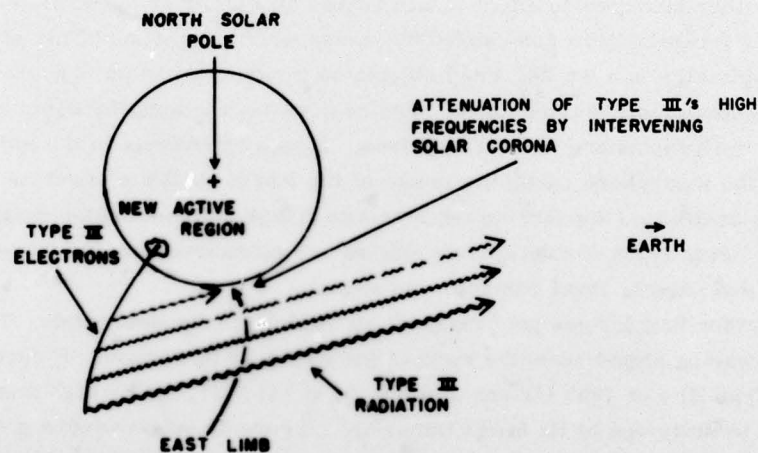


Figure 48. Geometry of Pre-Limb Dekameter Burst Activity With Respect to Earth Observation

Several days before the region reaches the limb the dekameter SFIR will begin recording fuzzy Type III's, groups of III's and V's. These bursts will be limited to the lowest frequencies.

One or two days before optical limb or coronagraph observation, the SFIR may record activity to 75 MHz but with some weakening of signal at the 75-MHz end. A noise storm may commence on the 245- through 410-MHz discrete frequency radiometers at the end of this period. Type II's and IV's may be observed without optical correlations during this period.

The day before optical disk observation, large bursts at 610, 1415, 2695, and 4995 MHz will normally be evident. As the day progresses, the higher frequency radiometers begin recording bursts.

As the 8800 and 15,400 MHz radiometers begin recording weak burst activity, optical activity will be observed.

4.7 Total Power Trace Signatures

The total power (TP) output of the SFIR can also be used to determine burst types. Figure 49 illustrates schematically the different burst type signatures as they appear on the total power channel. Figure 49 should only be used as a generalized example. The relative intensities of the six signatures are not representative. The figure was only meant to convey the general shape.

The Type II TP signature is generally typified by a rapid start and a duration of several minutes. Type II's cannot be unambiguously identified using the TO.

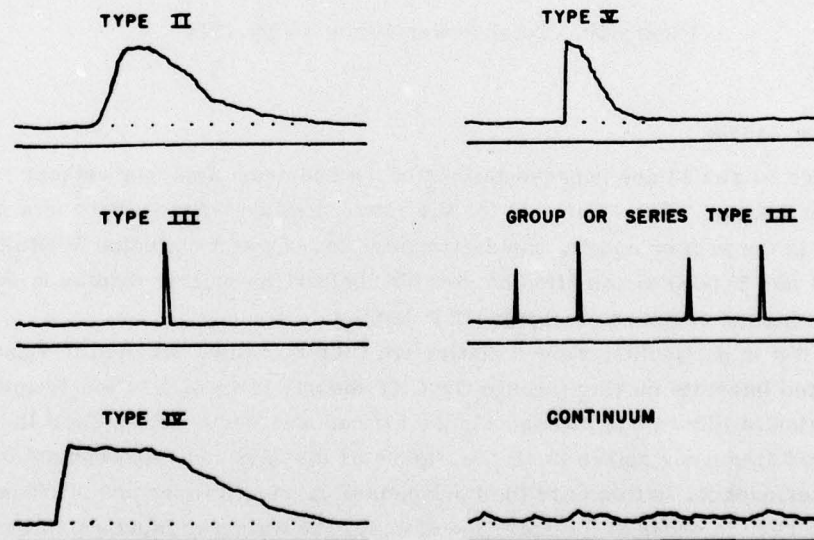


Figure 49. Typical Total Power Signature

The Type V can be identified with the TP trace, since the sharp rise and tapered ending are unique to Type V's when it is combined with a duration of tens of seconds to a few minutes. Type V's are also the most intense frequently observed bursts.

Type III's and groups of III's are unambiguously identified by their short duration.

Type IV's and continua can sometimes be differentiated by their intensity fluctuations. Type IV's should show very little intensity fluctuation after onset, whereas continua show a rough intensity trace that usually returns to the pre-burst level during the continuum. Type IV's, on the other hand, will only return to the pre-burst level at the end of the burst.

Figure 50 is the intensity profile that corresponds to Figure 43. Note that the intensity profile of an actual burst is a composite of several types and more difficult to interpret than the simplified schematic of Figure 49.

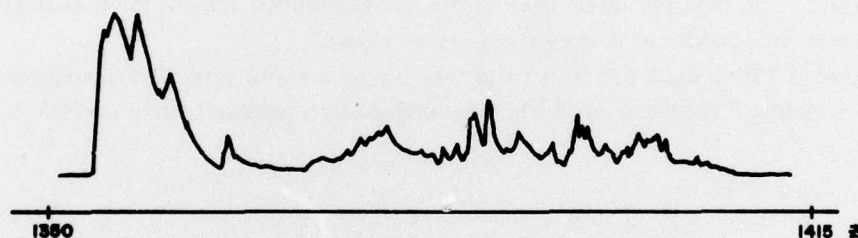


Figure 50. Total Power Trace 4 July 1974

4.8' Spectrum Analysis

Figures 51 and 52 are representations of the spectrum analyzer cathode ray tube (CRT) display. (See Figure 10 for the actual display.) Since there is a 10 - 15 min delay in the printer output, rapid determination of event criterion SFIR data (Type IV's and Type II's) can often be resolved before the printer display is available, by using the spectrum analyzer CRT display.

Type II's in particular, show a distinctive CRT signature depicted in Figure 51. The elevated intensity moving through the CRT display from high to low frequencies as illustrated in Figure 51a through Figure 51f can only occur with a Type II. The two constant frequency spikes in all the Figure 51 displays indicate constant background interference, in this case the fundamental carrier frequencies of channels 2 and 4 on TV. In order to interpret the display, the observer must watch the CRT through many sweeps (tens of seconds) since the motion of the elevated CRT trace is not apparent over a few seconds' observation.

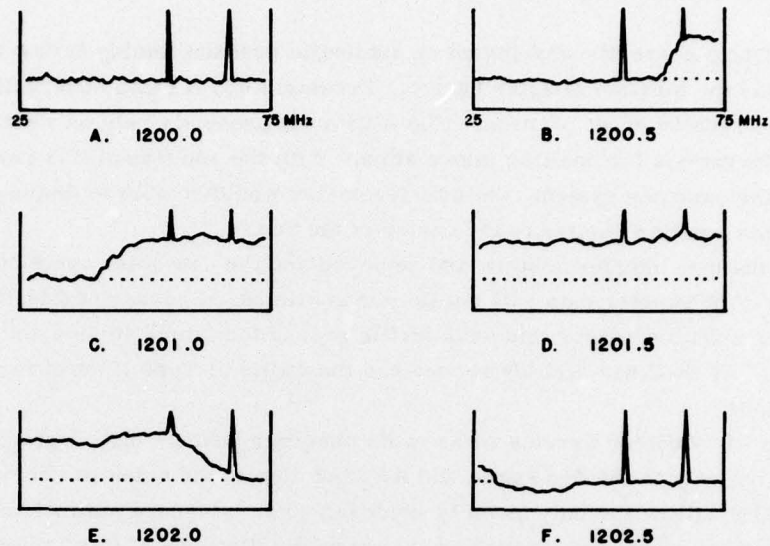


Figure 51. Instantaneous Spectrum Analyzer Display Type II

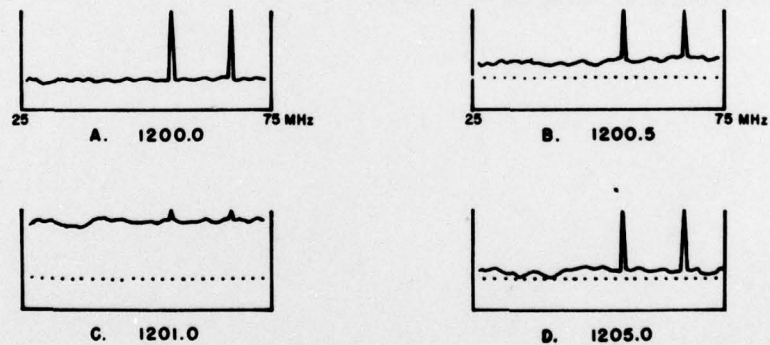


Figure 52. Instantaneous Spectrum Analyzer Display Type IV

Type IV's are also discernable by using the CRT as illustrated in Figure 52. Type IV's show a broad band elevation of the CRT display with no clear cut movement in frequency. The elevated levels will remain constant over tens of seconds after the initial turn on which distinguishes the burst from a continuum which will show rapid intensity changes over a few seconds distributed randomly in frequency.

5. FUTURE DEKAMETER/METER DEVELOPMENTS

AFGL is currently working on an automatic position finding device that will determine the location of solar bursts. Presently RSTN radio observations are unable to resolve event position. The AWS must presently rely on weather-dependent observations for position information. With the addition of this new device and another antenna system, the interferometer would be able to display a two-coordinate position related to the center of the Sun.

As the new interferometers are deployed and the new solar cycle begins, the quantity of dekameter data will multiply many times. Because of this, the solar observer should consider this area fertile ground for future studies and technical reports. AFGWC has already recognized the utility of Type II burst for proton predictions.

The Air Weather Service solar radio observer bears a high degree of responsibility not only to the Air Force and AWS but also to the scientific community. The AWS RSTN will be the only globally-deployed solar telescope network in existence with identical equipment throughout the network. Because of this, scientists will be using SFIR data supplied by the AWS as a baseline and fundamental comparison reference for inter-observatory data comparison. Reliable and scientifically accurate observations may lead to a better understanding of solar processes through improved theoretical modeling of the Sun.

Bibliography

NOTE: The authors would like to recommend the report written by G. L. Tarnstrom in particular, for those interested in a better theoretical understanding of solar radio astronomy.

Tarnstrom, G. L. (1974) Introduction to Solar Radio Astronomy, University of Oulu, Oulu, Finland ISBN 951-42-0211-2, 19.

Alvarez, H., and Haddock, F. T. (1973) Solar Phys. 29:197.

Boischot, A., De la Noe, J., and Moller-Pedersen, B. (1970) Relation between metric and decametric noise storm activity, Astron. & Astrophys. 4:159-160.

De Jager, C. (1970) in E. R. Dyer (ed), Solar Terrestrial Physics, Part I, D. Reidel Publishing Co., Dordrecht, 1.

De la Noe, J., Boischot, A., and Aubier, M. (1973) in R. Ramaty and R. G. Stone (eds.), High Energy Phenomena on the Sun, NASA-GSFC, Greenbelt, Maryland, 602.

De la Noe, J. (1974) On the probability of occurrence of the type IIb burst as a precursor, Solar Phys. 37:225-233.

Elgaroy, O. (1961) Astrophys. Norvegica 7:123.

Fainberg, J., and Stone, R. G. (1974) Satellite observations of type III solar radio bursts at low frequencies, Space Science Reviews, 16:145-188.

Gaunt, D. N. (1976) The Sagamore Hill Sweep Frequency Interferometric Radiometer Used for Solar Studies in the Dekametric Band, AFGL-TR-76-0194.

Gordon, I. M. (1971) Astrophys. Letters 5:521.

Hanasz, J. (1966) Australian J. Phys. 19:635.

Hanasz, J. (1968) Chains of type I solar radio bursts, Aus. J. Phys. 19:635-47.

Bibliography

- Kai, K. (1970) The structure, polarization, and spatial relationship of solar radio sources of spectral types I and III, Solar Phys. 11:456-466.
- Kraus, J. D. (1966) Radio Astronomy, McGraw-Hill, New York.
- Kundu, M. R. (1965) Solar Radio Astronomy, Wiley Interscience, New York.
- Lee, R. H., and Warwick, J. W. (1964) Radio Science, 68D:807.
- Malville, J. M. (1962) Astrophys. J. 136:266.
- Maxwell, A., and Swarup, C. (1958) Nature 181:36.
- Maxwell, A., and Thompson, A. R. (1962) Astrophys. 135:138.
- Melrose, D. B. (1974) Solar Phys. 35:441.
- Parker, E. N. (1958) Phys. Res. 109:1328.
- Parker, E. N. (1963) Astrophys. J., Supplement 8:177.
- Parker, E. N. (1973) Plasma Phys. J. 9:49.
- Pawsey, J. L. (1950) Proc. IEE, Part III, London, 97:290.
- Payne-Scott, Ruby, and Little, A. G. (1951) Australian J. Sci. Res. Series A, 4:508.
- Petschek, H. E. (1964) in W. N. Hess (ed.), AAS-NASA Symp. on the Physics of Solar Flares, NASA-SP-50.
- Ramaty, R., and Petrosian, V. (1972) Astrophys. J. 178:241.
- Smerd, S. F., Wild, J. P., and Sheridan, K. V. (1962) Australian Phys. J. 15:180.
- Smith, D. F., and Sturrock, P. A. (1971) Astrophys. Space Sci. 12:411.
- Smith, D. F. (1970) Solar Phys. 15:202.
- Smith, D. F. (1974) Solar Phys. 34:393.
- Smith, D. F. (1974) Space Sci. Res. 16:91.
- Solar Radio Group UTRECHT (1974) Type III bursts, Space Sciences Reviews, 16:45-89.
- Stewart, R. T. (1974) Solar Phys. 39:451.
- Stewart, R. T. (1975) An example of a fundamental type IIIb radio burst, Solar Phys. 39:451.
- Stone, R. G., and Fainberg, J. (1971) Solar Phys. 20:106.
- Sturrock, P. A. (1964) in W. M. Hess (ed.), AAS-NASA Symposium on the Physics of Solar Flares, NASA-SP-50:357.
- Swarup, G., Stone, P. H., and Maxwell, A. (1960) Astrophys. J. 131:725.
- Takatura, T. (1963) Publ. Astron. Soc. Japan, 15:462.
- Takakura, T., and Yousef, S. (1975) Type IIIb radio bursts: 80 MHz source position and theoretical model, Solar Phys. 40:421-438.
- Tsytovich, V. N. (1970) Nonlinear Processes in a Plasma, Plenum Press, New York.
- Warwick, J. W. (1965) Sweep-Frequency Measurements of Solar Bursts in Solar System Radio Astronomy, Ed. J. Aarons, Plenum Press, New York.
- Weiss, A. A. (1963) Australian J. Phys. 16:526.
- Wild, J. P. (1950) Australian J. Sci. Res. A3:541.

Bibliography

- Wild, J. P., Smerd, S. F., and Weiss, A. A. (1963) Ann. Rev. Astron. Astrophys. 1:291.
- Wild, J. P., and Smerd, S. F. (1972) Ann. Rev. Astron. Astrophys. 10:159.
- Zirin, H., and Lazareff (1975) Sunspot motion flares and type III bursts in McMath 11482, Solar Phys. 41:425-438.